UNIVERSITAT DE BARCELONA

Field-effects on single molecular circuitry

Electronic transport from synthetic to biological models

Albert Cortijos i Aragonès

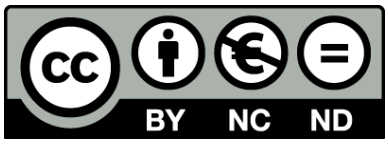

Chapter 3

Mimicking natural structures: Metalloporphyrins

Porphyrins are one of the most extended molecular structures involved in a wide variety of important biological processes ranging from the activation and the transport of molecular oxygen in mammals[371–375] to harvesting of sunlight in plant photosynthetic systems[371,373–377] or even from catalysis to pigmentation changes.[378,379] Porphyrin-based fundamental biological representatives include hemes, chlorophylls, vitamin B-12 and several others.[378–390] Heme proteins (containing Fe) serve many roles,[381–386,389] like O_2 storage and transport (myoglobin and hemoglobin),[382,383] electron transport[384,385] (Cytochromes b and c) as well as O_2 activation and its utilization (Cytochrome P450 and cytochrome oxidase).[375,386,387] Chlorophylls[388,390] (which have a central Mg ion) and pheophytins[389] (which are metal free) are found in the photosynthetic apparatus of plants and bacteria, while vitamin B-12 (which has Co)[378] is catalytically active in many bacterial species and animals.

But, how is a metalloporphyrin molecule' Mainly, these molecules basically are conformed by a macrocycle (the porphyrin ring) which consists of four pyrrolic ringed subunits bridged by four (meso) carbon atoms (see Figure 3.1). This macrocycle is an extraordinarily chemically stable aromatic system, and the nitrogen atoms at the interior form a central pocket ideally positioned to firmly incorporate metal atoms in a tetradentate fashion, the size of which is perfect to bind in the cycle cavity almost all metal ions and, indeed, a large number of metals can be inserted in the center of the macrocycle forming metalloporphyrins like Fe, Co, Ni, Cu, Cr, Mn or Zn providing the different properties.[191,391–394] Metalloporphyrin' structural flexibility and well-developed synthetic chemistry allows their chemical and physical properties to be tailored by choosing from an extensive variety of macrocycle substituents along the central metal atoms, making them very attractive for producing highly functional materials with a huge variety of applications. Metalloporphyrins are usually employed as additives in organic layers or used as structural units by themselves, controlled using different supramolecular chemistry techniques, obtaining diverse arrays of nano- or microscale organized blocks habitually built-up using

self-assembled methods.[395–397]

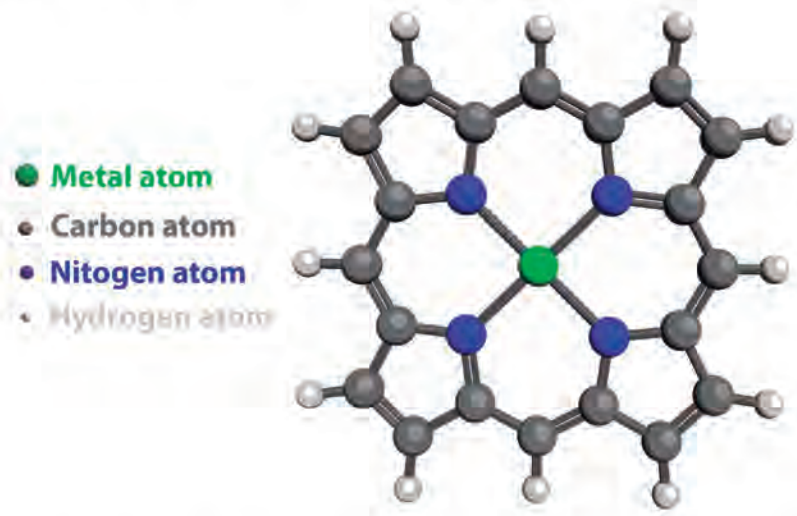

Figure 3.1: Representation of a simple metalloporphyrin, atoms are labeled on the figure.

Metalloporphyrins' anionic cavities represent coordinatively unsaturated units for charge transfer and ligation of adducts, which occurs with reversible changes of electronic configuration, and is the main reason of their extended use as biostructures. Inspired by these functionalities observed in nature, technology-based found several applications mimicking them and incorporating in different fields. Given the capabilities of metalloporphyrins to bind and release gases and to act as active centers in catalytic reactions of biological systems, metalloporphyrin-based films on surfaces have been vastly used, representing the most novel synthetic biomimetic devices. Their use is extremely appealing as chemical and gas sensors[398] and also have been introduced in nonporous catalytic materials.[399,400] Moreover, the role of metalloporphyrins in photosynthetic mechanisms indicates a good attitude of these molecules to mediate photon-electron energy transfer processes[401] due to their highly conjugated porphyrin rings combined with a well-defined and strong absorption in the visible spectrum,[402] reason why in recent years the interfaces between metalloporphyrins and suitable substrates (specially Si, TiO_2 and noble metals) have become of major interest for applications, such as in opto-electronics as well as data storage[403,404] and also in a still increasing number of covalently linked donor-acceptor supramolecular metalloporphyrin based assemblies.[405,406] Particularly in optoelectronics field, metalloporphyrins have attracted much attention at the nanoscale level, overall in solar cells applications due the inherent intense and absorption bands tunable through the metal centers.[334,407–409] Examples of such applications are organic thin film transistors (OFETs),[410] organic light emitting diodes (OLEDs),[411,412] organic semiconductors (OSCs)[411–415] and organic photovoltaic devices (OPVs).[416]

The main objectives of this chapter are two. The first is the development of a robust platform which allows the highest efficiency for the electron transport, through

a single-molecule device based on metalloporphyrins molecules. This platform also will be used to perform an exhaustive study of the electron transport phenomenology presented by such metalloporphyrins molecular wires, aimed to establish the basis of the conductance measurements thus allowing the proper development of the second objective, which is the design of a single-molecule spin-filter device gathering all the concepts figured out at the previous chapter.

3.1 Metalloporphyrins as molecular circuitry platforms

Focusing on the molecular-scale, metalloporphyrins offer a huge variety of desirable features as building blocks for future molecular-scale devices thanks to gathering different properties such as a highly-conjugated structure[417,418] with a very narrowed length-conductance attenuation factor ($0.04\mathring{A}^{-1}$),[376,419] rigid planar geometry,[420–422] highly chemical stability[423,424] and the capability to form stable junctions with different stable conformations[425,426] by easily coordinating them through the porphyrin ring's substituent[53,85,300,419,427,428]

Crucial to further development for future single-molecule applications based on metalloporphyrins, is imperative the nanoscale understanding of the interactions that occur at the molecule-electrode interface[429–431] as well as their charge transfer processes. Regarding the molecule-electrode interactions, the dependence of the electronic and conformational structures on the adsorption, has been vastly studied using very different techniques such as the STM,[198,376,425,426,432] the UV photoemission spectroscopy,[433] and XPS,[434] and also from the computational field with DFT applications.[435] Several studies have shown that single-molecule conductance measurements can be significantly affected by the binding geometry,[436] the coupling of the π orbitals with the metallic leads,[437] or the π-π stacking between adjacent molecules,[438] like the well-known and widely studied J- and H- aggregates presented by porhyrins.[439–445] About the charge transport properties, many metalloporphyrin derivatives and oligo-porphyrins junctions[376,446,447] have been studied experimentally and theoretically, and some interesting electronic properties have been revealed, such as long-range electron tunneling on junctions,[419] current switching,[448] field-effect characteristics, photo-induced electron transfer[449–452] and even current rectification.[453]

From the extended research above presented, can be extracted the crucial importance of the molecular interactions with the electrodes due the caused effects over the conformation and the need to control it. Up to now, the conformation employed in all the reported metalloporphyrins' single-molecule conductance measurements, were based on a porphyrin ring stacked perpendicular to the electrodes thus parallel to the direction of electron-pathway (see left panel of Figure 3.2). This upright configuration, is the most common molecular plane orientation since the direct strong attachment of the metalloporphyrins' substituent to the electrodes due the established high affinity.[53,376,419,454,455] Unfortunately, metalloporphyrin junctions under the such upright configuration are highly affected by several phenomenon, being the

most representative the molecule-electrode interactions dependence to the used anchoring groups[53,85,376,419,454–456] due their possible multiple-contact geometries and specially the π-orbitals coupling to the metallic leads. They represent significant limiting factors which should be taken in account to perform single-molecule devices for future applications, converting the junctions based on metalloporphyrins as a drawback for its development.

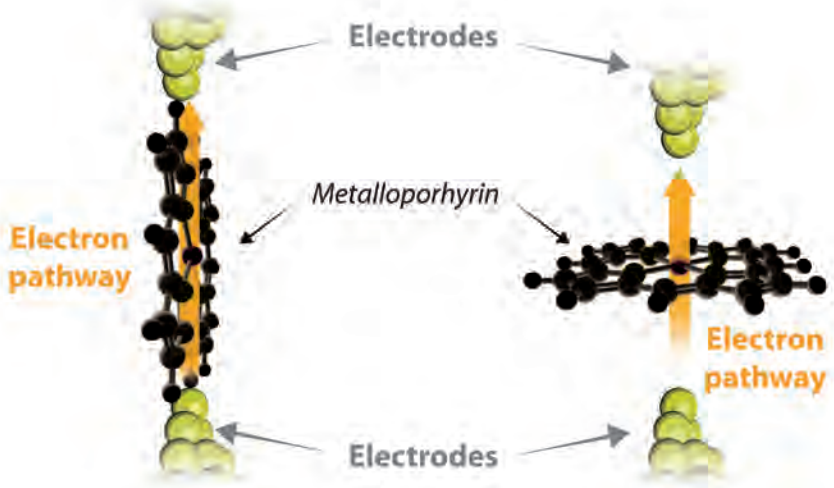

Figure 3.2: Representation of a metalloporphyrin under the upright configuration parallel to the electron-pathway (left) along with the flat conformation perpendicular to the electron-pathway (right).

Inspired by all the previous works, in this section is proposed the development of a new single-molecule approach with the highest efficiency for the electronic transport employing metalloporphyrins, thereby preventing from all the explained drawbacks inherent to the common upright configuration (see left panel of Figure 3.2). In order to carry it out, was mimicked the natural way to orient the metalloporphyrin structures[371,372,375,457] easily found in photosynthetic biological processes or the respiratory chain, between many other electron transfer processes.[371,375,458] In such scenarios, the plane of the metalloporphyrin porphyrin ring is perpendicular aligned to the direction of the electron transport (see right panel of Figure 3.2) (therefore parallel to the electrodes in a junction), reducing significantly the effect of parasitic phonons thanks to a transport directly via the metal.[457,458] To study this new approach to perform molecular junctions based on a metalloporphyrin flat conformation, the proposed experiments will consist on single-molecule conductance experiments STM-BJ technique and performed under RT conditions as is detailed at the next section.

3.1.1 The experimental research

The aim of this section was to combine within the STM, all the needed ingredients to achieve a molecular junction which allows the electron transport through a metalloporphyrin via a direct conduction through its metal center thanks to the perpendicular molecular plane (flat conformation) respect the electron-pathway. In previous works, the molecular metalloporphyrins had been linked to the Au electrodes using several terminal groups as anchoring groups like sulfonate ($-SO_3^-$), hydroxyl (-OH), nitrile (-CN), amine ($-NH_2$), carboxylic acid (-COOH), benzyl ($-C_6H_6$), or pyridyl ($-C_6H_5N$)..[53,82,85,454,456] Inspired by them, in the presented study in order to achieve the desired "*lying*" flat conformation were used pyridin-4-yl-methanethiol (*Pyr*) molecules (see Figure 3.3) synthesized according to Puigmartí and co-workers.[459] *Pyr* molecule is a very convenient linker to ensemble supramolec-

Figure 3.3: Chemical structure of pyridin-4-yl-methanethiol molecule used to functionalize Au electrodes, alongside a model representation

ular structures perpendicular to the surface[460,461] with a reduced mobility (therefore stability) and also with a high efficiency for the molecular trapping.[462] In the presented single-molecule device, *Pyr* molecules functionalized the electrodes attached via the -S terminus (thiol) due the well-known S-Au affinity,[463–467] therefore the non-linked -N terminus (pyridine),[459] is available to interact axially with the metal center because of the strong N-metal affinity.[85,468–472] Tip and substrate electrodes axially linked to the metal center, afforded a hexacoordinate system (see Figure 3.4 panel right)[85,473–475] connecting the metalloporphyrins in a parallel conformation allowing a stable junction with the aim to close the circuit between both electrodes.

The selected technique was STM-BJ (see *Section "STM Break-Junction Technique"*, on Page 26) employed at RT and the experiments were carried out employing polycrystalline Au wire to obtain the STM tips electrodes as well as the Au(111) monocrystals were utilized as substrate electrodes, the used medium was mesitylene organic solvent. The measured molecules were Co(II)-5,15-diphenylporphyrin (Co-DPP) (see Figure 3.5) metalloporphyrin which was synthesized according to the procedure described by Song et al.[476,477] Besides, as a control molecule was used the free base porphyrin, 5,15-diphenylporphyrin (DPP), since it has no metal center

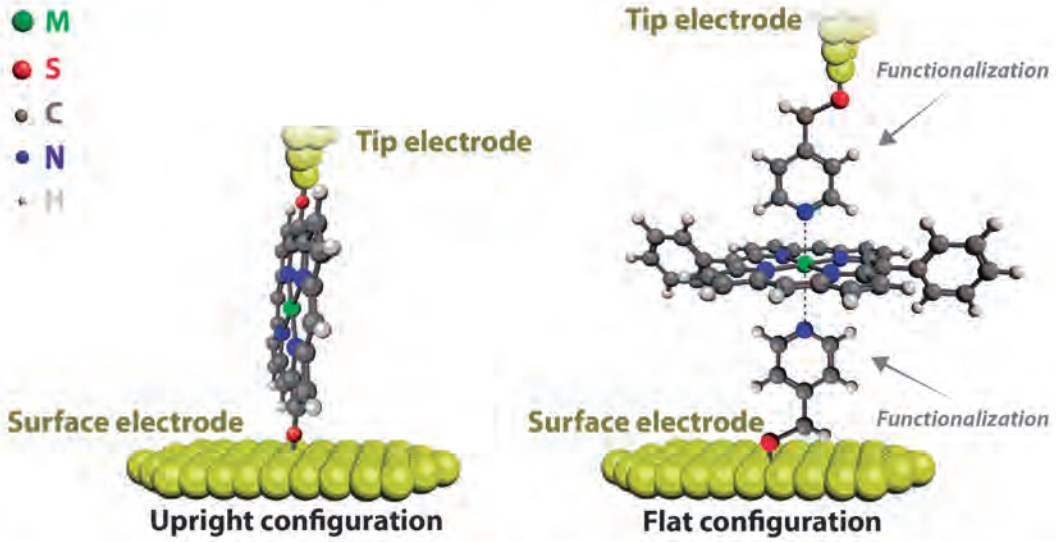

Figure 3.4: Schematic representations of the common upright configuration (left) for single porphyrin conductance experiments and the flat configuration investigated in this study (right).

it was employed with the aim to confirm the observed conductances to junctions due the metal interaction with the N-*Pyr*. A detailed description of the sample, substrate and tip preparation can be found from Page 328 (*Appendix C.2*).

Figure 3.5: Representation of the Co-metalloporphyrin (Co-DPP) used in this study, atoms are labeled on the figure.

The employed approaches were the already used "dynamic" *tapping* and "static" *blinking* (see *Appendix C.1*, Page 325). The former was used to capture in a very robust way, thousands of junction currents decays during the tip retraction to allow the statistical determination of the trapped molecule's conductance values. Despite the drawbacks associated to the upright configuration should not be present, also was needed to study the possible contact geometries inherent to any junction, for this reason was used the *blinking* approach to study the effects of the molecular

conformations through different tip-substrate electrodes distances in a static and motion-less way, letting the molecule to attach in a spontaneous way preventing from any undesirable mechanical contribution to the system.

The performed single-molecule conductance measurements were supported by computational calculations on gas phase for the *Pyr*-Co-DPP-*Pyr* and *Pyr*-DPP-*Pyr* adducts with the aim to reproduce the junction structures, as well as the isolated DPP was studied as reference. The employed methods were based on DFT within the B3LYP approximation, including effective core potentials with relativistic effects (In order to consider heavy metal atoms) and accounted by using a *LANL2DZ* basis set. The aim was the optimization of all the possible geometries for the molecular conformations together with the distribution of the frontier HOMO-LUMO orbitals. Due the significant high dihedral angle of ca. 81° between the phenyls and the porphyrin, is caused an electronic decoupling of the former, therefore the phenyl groups present a lack on electronic contribution to the molecular orbitals involved in the transport process and for simplicity they have been removed from geometry optimizations.[44]

3.1.2 Objectives and Summary of the experimental work

- The dynamic STM-BJ *tapping* approach was used to determine the molecular conductance of the Co-DPP molecule. The single-current measurements were performed under +5 mV of bias voltage.

- To study the origin of the multiple observed currents signatures and to associate them to spontaneous different contact geometries, were applied the *blinking* approach thereby avoiding any mechanically induced effect. These static experiments were done at +5 mV of bias voltage and to evaluate the effect of the tip-surface gap distance, were chosen large, intermediate or small separations corresponding to the 2, 4 and 9 nA set-point values of current, respectively.

- To ascertain unequivocally the establishment of a molecular junction between the two electrodes during the *blinking* experiments, was applied a control routine based on exerting mechanical pullings over the *blinking* events in different occasions assessing the molecular junction thanks to the observed of small plateaus. For a more detailed description of this procedure see *Appendix C.1* (Page 325).

- *Tapping* and *blinking* single-conductance experiments were performed to DPP molecules under the same conditions used with the Co-DPP to compare the obtained current signatures for both sets of experiments.

- *Blinking* control experiments were performed in the absence of DPP or Co-DPP, with both Ni tip and substrate functionalized with *Pyr* groups. Also were performed in the opposite way, in the absence of the *Pyr* units at the Ni tip and substrate electrodes and with Cu-DPP molecules present in solution. Both sets of current experiment were done to confirm all the current signatures to the bonding between de Co-DPP and DPP and the N-*Pyr*.

In the following pages is shown summarized the research as a published paper and its Supplementary Information:

"Albert C Aragonès, Nadim Darwish, Wojciech J Saletra, Lluïsa Pérez-García, Fausto Sanz, Josep Puigmartí-Luis, David B Amabilino, and Ismael Díez-Pérez. Highly conductive single-molecule wires with controlled orientation by coordination of metalloporphyrins. *Nano letters*, 14(8):4751–6, aug 2014".

NANO LETTERS
Letter
pubs.acs.org/NanoLett

Highly Conductive Single-Molecule Wires with Controlled Orientation by Coordination of Metalloporphyrins

Albert C. Aragonès,[†,‡,¶] Nadim Darwish,[†,¶] Wojciech J. Saletra,[§] Lluïsa Pérez-García,[∥,⊥] Fausto Sanz,[†,‡] Josep Puigmartí-Luis,*[,§,#] David B. Amabilino,*[,§] and Ismael Díez-Pérez*[,†]

[†]Departament de Química Física, Universitat de Barcelona, Diagonal 645, and Institut de Bioenginyeria de Catalunya (IBEC), Baldiri Reixac 15-21, 08028 Barcelona, Catalonia, Spain

[‡]Centro Investigación Biomédica en Red (CIBER-BBN), Campus Río Ebro-Edificio I+D, Poeta Mariano Esquillor s/n, 50018 Zaragoza, Spain

[§]Institut de Ciència de Materials de Barcelona (ICMAB-CSIC), Campus Universitari, 08193 Bellaterra, Catalonia, Spain

[∥]Facultat de Farmàcia, Universitat de Barcelona, 08028 Barcelona, Catalonia, Spain

[⊥]Institut de Nanociència i Nanotecnologia, Universitat de Barcelona, 08028 Barcelona, Catalonia, Spain

[#]Empa, Laboratory for Protection and Physiology, Lerchenfeldstrasse 5, 9014 St. Gallen, Switzerland

Supporting Information

ABSTRACT: Porphyrin-based molecular wires are promising candidates for nanoelectronic and photovoltaic devices due to the porphyrin chemical stability and unique optoelectronic properties. An important aim toward exploiting single porphyrin molecules in nanoscale devices is to possess the ability to control the electrical pathways across them. Herein, we demonstrate a method to build single-molecule wires with metalloporphyrins via their central metal ion by chemically modifying both an STM tip and surface electrodes with pyridin-4-yl-methanethiol, a molecule that has strong affinity for coordination with the metal ion of the porphyrin. The new flat configuration resulted in single-molecule junctions of exceedingly high lifetime and of conductance 3 orders of magnitude larger than that obtained previously for similar porphyrin molecules but wired from either end of the porphyrin ring. This work presents a new concept of building highly efficient single-molecule electrical contacts by exploiting metal coordination chemistry.

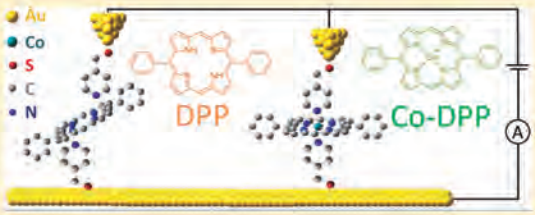

KEYWORDS: *single-molecule wires, coordinating individual metalloporphyrins, controlled molecular orientation, optimized coupling by axial coordination*

Inspired by the proposal that single molecules will be functional parts of future electronic devices, there exists a considerable interest in understanding charge transport across them, both experimentally and theoretically.[1−8] One of the numerous molecular systems that hold great promise in this area is porphyrins, partly because of their well-developed synthetic routes by which a variety of chemical substituents and central metal ions can be introduced in their structure to tune their electrical properties. Porphyrin derivatives play a vital role in charge separation that take place in naturally occurring photosynthetic processes and in metalloproteins involved in the respiratory chain,[9−13] and it is envisioned that they can play an important role in future artificial electronic devices.[14−16] For these reasons, it is critical to understand and control charge transport through porphyrins, which is a process largely dictated by the electrode−molecule orientation and the porphyrin−electrode chemical contacts during measurements.

Recent studies using the scanning tunneling microscope (STM) break-junction technique[1] showed that the conductance of a single porphyrin covalently bond in an upright configuration is significantly affected by the binding contact geometry, the employed chemical anchoring groups and the coupling ability of the π orbitals to the metallic leads.[17−23] Porphyrin junctions in such a configuration were shown to exhibit unique characteristics such as a very shallow decay of conductance with length ($\beta = 0.04$ Å^{-1}).[17,18] In these previous studies, the supramolecular backbones of the porphyrins were modified synthetically to allow their attachment to the electrodes, usually gold, via a suitable linker such as thiols and pyridines.[19,20] The strong affinity of such contact groups to the gold electrodes together with the rigid structure of the porphyrin backbone is anticipated to yield restricted junction configurations. Thus, the configuration of the single-molecule junctions formed from porphyrins is commonly represented as being straight and perpendicular to the electrodes[17−21] (Figure 1a). These built-in chemical contacts were

Received: May 21, 2014
Revised: June 24, 2014
Published: June 30, 2014

   dx.doi.org/10.1021/nl501884g | Nano Lett. 2014, 14, 4751−4756

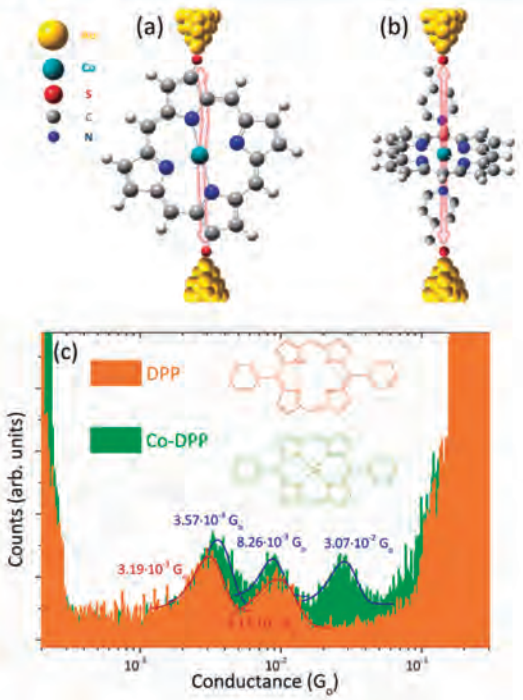

Figure 1. (a) Representation of the common upright configuration for single porphyrin conductance experiments. (b) Schematic representation of the flat configuration investigated in this work. (c) Semilog conductance histograms for the DPP molecule (orange) and Co-DPP molecule (green) using the junction configuration represented in panel b. The conductance values are extracted from Gaussian fits of the peaks.

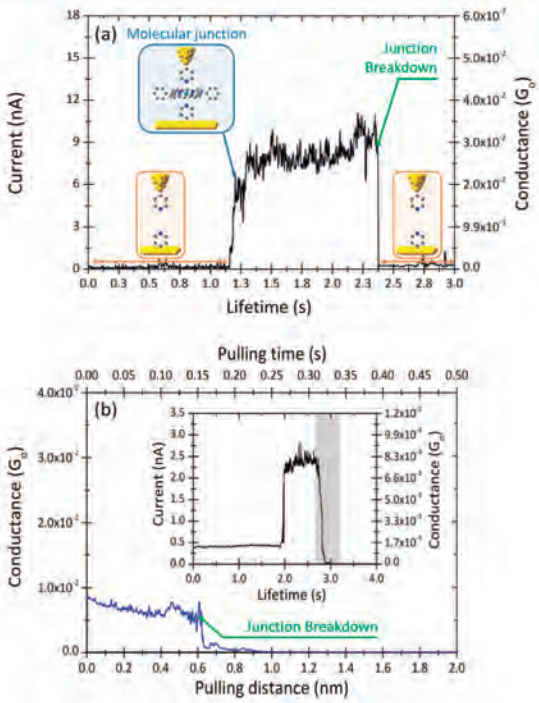

Figure 2. (a) Representative "*blink*" due to the spontaneous formation of a single-molecule junction with the Co-DPP molecule; the current decays suddenly due to either spontaneous or induced breakdown of the junction. Tip-to-sample distance was initially set by a 4 nA set point current and normalized to zero in the plot. (b) Shows an induced STM tip pulling curve of the inset blink (the shadowed area indicates the pulling stage) for the Co-DPP molecule.

successful for studying charge transport along the length of the porphyrin backbone and pave the way to the investigation of other interesting junction configurations such as the porphyrin oriented flat between the electrodes. Such a new configuration mimics the electron transport across porphyrins in naturally occurring phenomena such as photosynthetic and transmembrane electron transport.[11,12] In these natural processes, the common orientation of the porphyrin ring is perpendicular to the main pathway of electrons or energy through an axial coordination of chemical ligands with the metal center of the porphyrin molecule.[12,13]

In this study, we present a new approach to form single molecular junctions with porphyrin molecules. Namely, we chemically modify both the gold STM tips and Au (111) surfaces with pyridin-4-yl-methanethiol allowing porphyrin molecules introduced in the solution to close the circuit between the STM tip and the gold surface through metal−pyridine coordination (Figure 1b). We utilize the STM junction technique in its two common approaches, break-junction[1] and spontaneous formation of molecular junctions,[24] to determine the single molecular conductance. Further, we investigate the effect of the tip−surface distance on the conductance magnitude and the duration (lifetime) of the molecular junctions. We then propose molecular models that describe the experimental findings based on DFT optimized geometries and distribution of frontier orbitals of the most stable molecular configurations between the electrodes.

Two molecules were used in this study, a free base porphyrin, 5,15-diphenylporphyrin (DPP), which has no metallic center and therefore no strong interaction with the pyridinyl groups on the electrode surfaces, and a metalloporphyrin Co(II)-5,15-diphenylporphyrin (Co-DPP) with a divalent cobalt center, which allows coordination[25] to pyridinyl ligands affording a hexacoordinate system.[26−28] Initially, the STM break-junction approach[1] was used to determine the single-molecule conductance of each molecule. Conductance histograms (Figure 1c) were built by the accumulation of hundreds of individual pulling traces and the peak maxima represent the most probable conductance values (see Supporting Information section 9 for details).

In the conductance histograms, both the DPP molecule and the Co-DPP share two conductance levels, a low conductance (**LC**) level at ca. 3×10^{-3} G_0 and a medium conductance (**MC**) level at ca. 9×10^{-3} G_0. Unlike the DPP molecule, the Co-DPP shows an extra high conductance (**HC**) level at ca. 3×10^{-2} G_0. This **HC** value is about 3 orders of magnitude higher than that obtained previously from porphyrin molecules of comparable length to the Co-DPP molecule, but directly connected to the electrodes in an upright configuration.[18,21]

In order to understand the origin of the multiple conductance peaks observed in the break-junction experiments of Figure 1c, we carried out current transient captures at a fixed distance such that spontaneous formation of molecular junctions is attained.

dx.doi.org/10.1021/nl501884g | *Nano Lett.* 2014, 14, 4751−4756

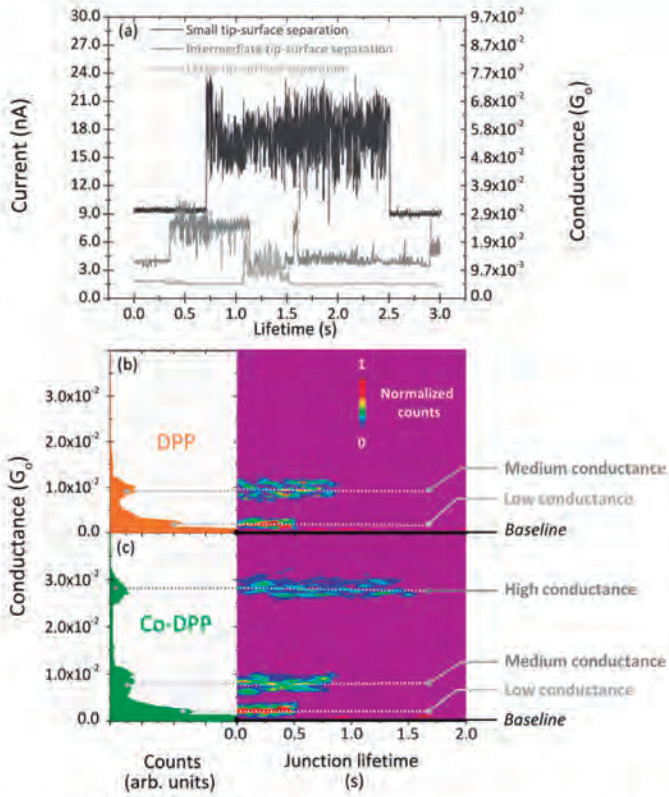

Figure 3. (a) Representative individual "*blinks*" corresponding to the formation of molecular junctions with the Co-DPP molecule at three different tip-to-surface distances determined by 2, 4, and 9 nA set point currents for large, intermediate, and small separations, respectively. (b,c) 1D conductance histograms (left panel) and the corresponding 2D maps (right panel) obtained from tens of *blinking* traces for (b) DPP and (c) Co-DPP. Counts (color legend) have been normalized versus the total amount of counts and a scale of one (100%) has been set for the maximum normalized value.

Briefly, imposing a set point tunneling current first sets an initial distance between the functionalized electrodes. The STM feedback is then turned off and the tunneling current is recorded as a function of time (Figure 2a). When a molecular junction is spontaneously formed, the current suddenly jumps. We refer to these current jumps as "*blinks*" and this type of experiments as the *blinking experiments*. The blink in this study corresponds to a molecular bridge formation between the pyridine-functionalized electrodes and the porphyrin molecule. The blinks typically last for a short period of time, after which the current suddenly drops due to the spontaneous breakdown of the junction. In order to ensure that the recorded blinks are due solely to the formation of molecular junctions, a mechanical induced STM tip pulling procedure[29] was eventually applied during the lifetime of the blinks (Figure 2b). The appearance of plateaus as the junction is mechanically forced to break evidence that the blink was due to the formation of a molecular bridge. Conversely, pulling the STM tip during the absence of a blink showed a fast exponential decay confirming the correlation between the appearance of blinks and the formation of molecular bridges (see details in Supporting Information section 1). Unlike the STM break-junction approach, which forces the tip in and out of the surface and therefore may lead to stretch-dependent conductance, the spontaneous formation of junctions (blinking approach) could be envisioned as a method to momentarily freeze particular conformations in the single-molecule junction.[24,30] More importantly, the blinking approach can provide reliable information about the lifetime and therefore the strength of the electrode-molecule interaction.

Typical blinking traces are shown in Figure 3a at different tip-to-surface separations. The statistical analysis of the measured conductances from the blinking traces is obtained from building 1D conductance histograms and 2D maps from tens of blinks (Figure 3b and 3c). Consistent with the values obtained from the STM break-junction experiments (Figure 1c), the DPP molecule showed **LC** and **MC** levels around 3×10^{-3} and 9×10^{-3} G_o, respectively. Likewise, the Co-DPP molecule showed, in addition to the **LC** and **MC** level, an extra **HC** level around 3×10^{-2} G_o. Note that the initial set point currents (baselines levels in Figure 3a) were set high (above 2 nA, see Supporting Information section 1) such as the tip and substrate are separated by short distances to promote "lying flat" conformations of the porphyrin between the electrodes, resulting in the measured high conductances (see control experiments in Supporting Information sections 3 and 4). The lifetime of the blinks was highest for the **HC**, followed by the **MC** and the shortest blinks were that for the **LC** (see details in Supporting Information section 2). The average lifetime of the **HC** blinks is 1.5 s at small tip-to-surface

dx.doi.org/10.1021/nl501884g | Nano Lett. 2014, 14, 4751−4756

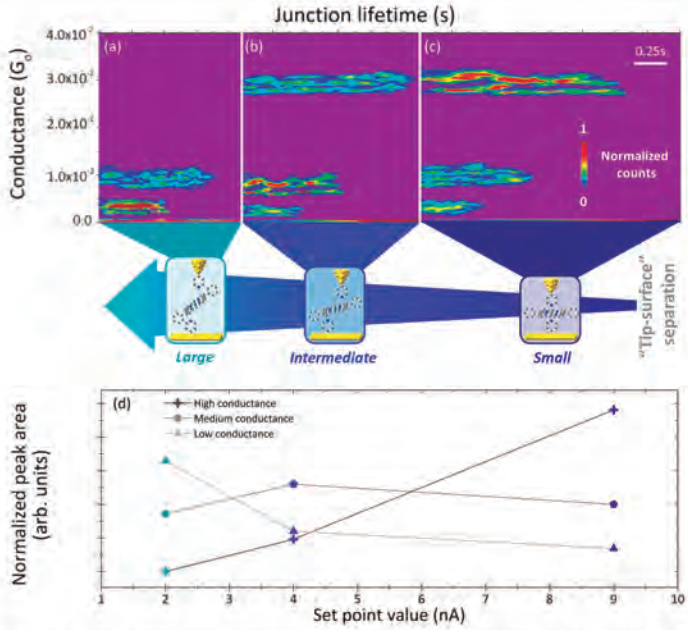

Figure 4. 2D *blinking* maps at three different tip-to-surface separations for the pyridinyl-coordinated Co-DPP junction at (a) large separation (2 nA set point current), (b) intermediate separation (4 nA set point current) and (c) small separation (9 nA set point current). The estimated decrease in the tip-to-substrate distance when going from (a) to (c) is ~0.9 nm (see Supporting Information section 1). (d) Plot of the normalized peak area of the 1D histograms in (a)–(c) (see Supporting Information section 5) versus current set point values (increasing set point means decreasing tip-to-surface separation). To allow comparison among (a)–(c), counts (color legend) have been normalized versus the total amount of counts among all three maps and a scale of 1 (100%) for the maximum normalized value has been set.

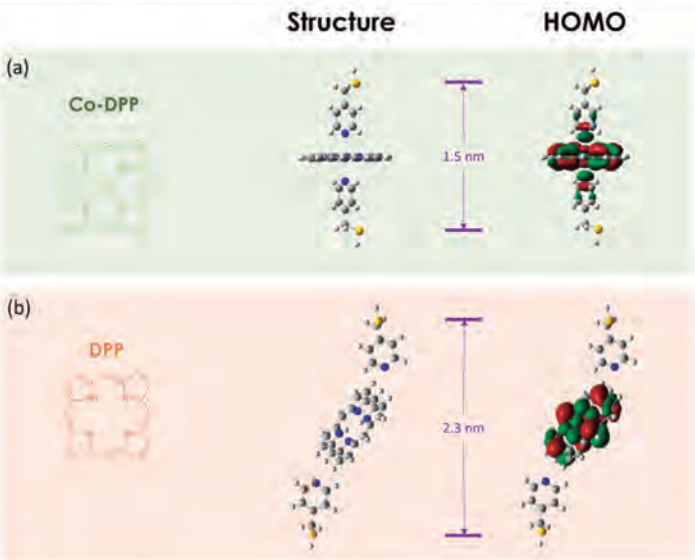

Figure 5. Molecular structure and DFT optimized geometry together with the HOMO frontier orbital of (a) the pyridine–Co-DPP–pyridine axial coordination and (b) the pyridine–DPP–pyridine coordination. The phenyl rings have been omitted for simplicity (see Supporting Information section 7).

gap distances, which suggests that the molecular junction configuration leading to the **HC** blinks are significantly more stable. Blinking experiments in the absence of porphyrin molecules or in the absence of the pyridinyl units at the electrodes showed no blinking events under the same experimental conditions (see details in Supporting Information

dx.doi.org/10.1021/nl501884g | *Nano Lett.* 2014, 14, 4751–4756

section 3 and 4). Thus, the presence of the **HC** level for the Co-DPP and its absence in the DPP in both the break-junction and the blinking experiments evidence that the Co center is directly involved in the molecular junction formation with Co-DPP molecules via hexacoordination of the Co metal center with the two nitrogen atoms in the pyridinyl units present on both the surface and the STM tip electrodes (Figure 1b). The transition from tetra to hexacoordinated Co with the two pyridine-modified electrodes gives rise to the extra high conductance level observed for the Co-DPP. Examples of similar high conductive molecular wires induced by a metallorganic redox moiety inserted into a molecular backbone have been previously reported.[31,32]

Further investigation of the origin of the three conductance levels (**LC**, **MC** and **HC**) was obtained by analyzing blinks for the Co-DPP molecule at different tip–surface gap separations. Figure 4a–c shows 2D maps built from tens of blinks recorded at different initial set point currents. The change in the number of bands (conductance levels) and their intensity (color counts) at the different set points indicates the propensity to stabilize particular molecular conformations as a function of the tip-to-surface separation. Namely, when the tip-to-surface separation is large, the most frequently observed blinks are the **LC** ones (see color counts in Figure 4a). As the tip-to-surface distance diminishes, the **MC** level dominates at intermediate distances, whereas the **HC** level dominates at the smallest separations (see color counts in Figure 4b–c and representative blinks in Figure 3a). The trends are observed by representing the normalized counts (see Supporting Information sections 5 and 6) of all three levels of conductance as a function of the tip-to-surface separation (Figure 4d). Note that the junction lifetimes are comparable for all three tip-to-surface separations, except for a slight (~0.25 s) increase in the **HC** junction lifetime when going from intermediate to small tip-to-surface separations. This last trend may suggest a partially strained hexacoordinated Co-DPP junction in the case of intermediate distances that results in premature force-induced junction breakdown decreasing the overall complex stability.

The distance-dependence of the **HC** blinks strongly suggests that they originate from molecular junctions through the cobalt coordination. Co coordination to the pyridine units requires the porphyrin molecule to be oriented flat at the junction (Figure 1b) with shorter pyridine-to-Co distance. Such a configuration is more likely to occur at small tip-to-surface separations (Figure 4c–d). This flat configuration is supported by geometry optimization of a pyridine–Co-DPP–pyridine junction using density functional theory (DFT-B3LYP) methods (see Supporting Information section 7), which revealed the formation of a hexacoordinated Co with the two pyridinyl moieties approaching the Co center at Co–N distances of less than 2 Å (Figure 5a center panel). This is consistent with the values obtained from X-ray crystal structures of Pyridine–Co–porphyrin–Pyridine complexes.[15] The strong Co–pyridine interaction is also demonstrated by the generation of delocalized HOMO orbitals along the pyridine–Co–pyridine axis (Figure 5a right panel). We attribute the **HC** level to the generated extended electronic pathway between the two electrodes by the molecular orbital delocalization along the junction main axis as a consequence of the pyridine–Co–pyridine coordination.

The **LC** and **MC** conductance levels that are common for both the DPP and the Co-DPP molecules can be explained by hydrogen bonding interactions between the pyridine units and the backbone of the porphyrin molecule that could happen at multiple sites. This hypothesis is supported by geometry optimization for the pyridine–DPP–pyridine adduct, which results in multiple configurations with the two pyridinyl groups forming H-bonds at different sites of the porphyrin (see representative H-bonding configurations in Figure 5b and Supporting Information section 7). Recent works have also suggested the possibility of wiring two electrodes through H-bonding interactions.[33,34] Hydrogen bonds can occur in geometries such that the porphyrin ring is highly tilted resulting in a much longer S-to-S junction (see Supporting Information section 7). These multiple long-distance interactions can be correlated with the dominance of the **LC** and the **MC** levels at larger tip-to-surface separations. The HOMO and LUMO levels of these H-bonding configurations are mostly localized on the porphyrin moiety (see Figure 5b right panel), with orbital-distribution similar to those obtained from the isolated porphyrin. The absence of delocalized orbitals along the pyridine–DDP–pyridine axis is an accord with the absence of **HC** level in the DPP junctions. The increase in the junction distance from Figure 5a to b is in qualitatively agreement with the estimated increase of tip-to-substrate distance when going from high to low set point values in Figure 4 (see Supporting Information section 1). It is important to note that in Figure 5b the electrode–electrode separation has been increased in the DFT optimization to identify possible interactions at large distances. However, H-bonding interactions can occur at a rather wide range between the H-donor and the H-acceptor[35] (Supporting Information Figure S6b top panel) and, therefore, H-bonding can also take place at the lower tip-to-surface separations such as that depicted in Figure 5a, as observed experimentally (see Figure 4c).

The approach outlined herein offers a control over the contact of porphyrin molecules in single-molecule circuitry such that previously inaccessible electronic pathways across the porphyrin can be achieved. This is made possible by "catching" the porphyrin molecule by its metallic center using coordination chemistry. We show that by changing the STM tip–surface distance we can alter the configuration of the junction and the binding sites and consequently control the conductance output of the single-molecule device. Of a particular note is the demonstration that by decreasing the STM tip–surface distance, the chances of wiring the porphyrin molecule from its metal center increase and, consequently, lead to a highly stable and highly conductive molecular wire. This high conductivity is attributed to the efficient electronic pathway via the metallic center of the porphyrin. We expect this general approach to be of a broader usage in the design of single-molecule devices that exploit coordination chemistry to achieve site-directed molecule–electrode connectivity.

■ ASSOCIATED CONTENT

Ⓢ Supporting Information

Experimental details on sample preparation and single-molecule transport experiments, control experiments of the single-molecule transport measurements and computational details. This material is available free of charge via the Internet at http://pubs.acs.org.

■ AUTHOR INFORMATION

Corresponding Authors

*E-mail: isma_diez@ub.edu.

*E-mail: amabilino@icmab.es.

*E-mail: josep.puigmarti@empa.ch.

Author Contributions

[‡]A.C.A. and N.D. contributed equally

Notes

The authors declare no competing financial interest.

■ ACKNOWLEDGMENTS

A.C.A. thanks the Spanish Ministerio de Educación, Cultura y Deporte for a graduate FPU fellowship. N.D. acknowledges the European Union for a Marie Curie IIF Fellowship. This research was supported by national projects CTQ2012-36090, CTQ2010-16339, and 2009 SGR 158 and EU Reintegration Grant (FP7-PEOPLE-2010-RG-277182). I.D.-P. and J.P.-L. thank the Ramon y Cajal program (MINECO, RYC-2011-07951 and RYC-2011-08071) for financial support.

■ REFERENCES

(1) Xu, B.; Tao, N. J. *Science* **2003**, *301*, 1221−1223.
(2) Nichols, R. J.; Haiss, W.; Higgins, S. J.; Leary, E.; Martin, S.; Bethell, D. *Phys. Chem. Chem. Phys.* **2010**, *12*, 2801−2815.
(3) Tao, N. J. *Nat. Nanotechnol.* **2006**, *1*, 173−181.
(4) Chen, F.; Tao, N. J. *Acc. Chem. Res.* **2009**, *42*, 429−438.
(5) Bürkle, M.; Viljas, J.; Vonlanthen, D.; Mishchenko, A.; Schön, G.; Mayor, M.; Wandlowski, T.; Pauly, F. *Phys. Rev. B: Condens. Matter Mater. Phys.* **2012**, *85*, 075417−12.
(6) Bürkle, M.; Zotti, L. A.; Viljas, J. K.; Vonlanthen, D.; Mishchenko, A.; Wandlowski, T.; Mayor, M.; Schön, G.; Pauly, F. *Phys. Rev. B: Condens. Matter Mater. Phys.* **2012**, *86*, 115304−8.
(7) Aradhya, S. V.; Venkataraman, L. *Nat. Nanotechnol.* **2013**, *8*, 399−410.
(8) Darwish, N.; Paddon-Row, M. N.; Gooding, J. J. *Acc. Chem. Res.* **2013**, *47*, 385−395.
(9) McDermott, G.; Prince, S. M.; Freer, A. A.; Hawthornthwaite-Lawless, A. M.; Papiz, M. Z.; Cogdell, R. J.; Isaacs, N. W. *Nature* **1995**, *374*, 517−521.
(10) Zhang, Z.; Huang, L.; Shulmeister, V. M.; Chi, Y. I.; Kim, K. K.; Hung, L. W.; Crofts, A. R.; Berry, E. A.; Kim, S. H. *Nature* **1998**, *392*, 677−84.
(11) Regan, J. J.; Ramirez, B. E.; Winkler, J. R.; Gray, H. B.; Malmström, B. G. *J. Bioenerg. Biomembr.* **1998**, *30*, 35−39.
(12) Gray, H. B.; Winkler, J. R. *Biochim. Biophys. Acta* **2010**, *1797*, 1563−72.
(13) Allen, J. W.; Watmough, N. J.; Ferguson, S. J. *Nat. Struct. Biol.* **2000**, *7*, 885−888.
(14) Liu, Z.; Yasseri, A. A.; Lindsey, J. S.; Bocian, D. F. *Science* **2003**, *302*, 1543−1545.
(15) Dey, S.; Ikbal, S. A.; Rath, S. P. *New J. Chem.* **2014**, DOI: 10.1039/C3NJ01248D.
(16) Lee, J. T.; Chae, D.-H.; Yao, Z.; Sessler, J. L. *Chem. Commun.* **2012**, *48*, 4420−4422.
(17) Sedghi, G.; Sawada, K.; Esdaile, L. J.; Hoffmann, M.; Anderson, H. L.; Bethell, D.; Haiss, W.; Higgins, S. J.; Nichols, R. J. *J. Am. Chem. Soc.* **2008**, *130*, 8582−8583.
(18) Sedghi, G.; García-Suárez, V. M.; Esdaile, L. J.; Anderson, H. L.; Lambert, J. C.; Martin, S.; Bethel, D.; Higgins, S. J.; Elliott, M.; Bennett, N.; Macdonald, J. E.; Nichols, R. J. *Nat. Nanotechnol.* **2011**, *6*, 517−523.
(19) Li, Z.; Smeu, M.; Ratner, M. A.; Borguet, E. *J. Phys. Chem. C* **2013**, *117*, 14890−14898.
(20) Li, Z.; Borguet, E. *J. Am. Chem. Soc.* **2011**, *134*, 63−66.
(21) Simbeck, A. J.; Qian, G.; Nayak, S. K.; Wang, G.-C.; Lewis, K. M. *Surf. Sci.* **2012**, *606*, 1412−1415.
(22) Perrin, M. L.; Prins, F.; Martin, C. A.; Shaikh, A. J.; Eelkema, R.; van Esch, J. H.; Briza, T.; Kaplanek, R.; Kral, V.; van Ruitenbeek, J. M.; van der Zant, H. S. J.; Dulic, D. *Angew. Chem.* **2011**, *123*, 11419−11422.
(23) Perrin, M. L.; Martin, C. A.; Prins, F.; Shalkh, A. J.; Eelkema, R.; van Esch, J. H.; van Ruitenbeek, J. M.; van der Zant, H. S. J.; Dulic, D. *Beilstein J. Nanotechnol.* **2011**, *2*, 714−719.
(24) Haiss, W.; Nichols, R. J.; van Zalinge, H.; Higgins, S. J.; Bethell, D.; Schiffrin, D. J. *Phys. Chem. Chem. Phys.* **2004**, *6*, 4330−4337.
(25) *Ionic Interactions in Natural and Synthetic Macromolecules*; Ciferri, A., Perico, A., Eds.; John Wiley & Sons, Inc.: Hoboken, NJ, 2012; p 337−359, DOI:10.1002/9781118165850.
(26) Corden, B. B.; Drago, R. S.; Perito, R. P. *J. Am. Chem. Soc.* **1985**, *107*, 2903−2907.
(27) Arnold, L.; Norouzi-Arasi, H.; Wagner, M.; Enkelmann, V.; Müllen, K. *Chem. Commun.* **2011**, *47*, 970−972.
(28) Wong, W.-Y. *Coord. Chem. Rev.* **2005**, *249*, 971−997.
(29) Diez-Perez, I.; Hihath, J.; Hines, T.; Wang, Z.-S.; Zhou, G.; Müllen, K.; Tao, N. *Nat. Nanotechnol.* **2011**, *6*, 226−31.
(30) Artés, J. M.; Díez-Pérez, I.; Gorostiza, P. *Nano Lett.* **2012**, *12*, 2679−84.
(31) Getty, S. A.; Engtrakul, C.; Wang, L.; Liu, R.; Ke, S.-H.; Baranger, H. U.; Yang, W.; Fuhrer, M. S.; Sita, L. R. *Phys. Rev. B: Condens. Matter Mater. Phys.* **2005**, *71*, 241401−4.
(32) Sun, Y.-Y.; Peng, Z.-L.; Hou, R.; Liang, J.-H.; Zheng, J.-F.; Zhou, X.-Y.; Zhou, X.-S.; Jin, S.; Niu, Z.-J.; Mao, B.-W. *Phys. Chem. Chem. Phys.* **2014**, *16*, 2260−2267.
(33) Zhao, Y.; Ashcroft, B.; Zhang, P.; Liu, H.; Sen, S.; Song, W.; Im, J.; Gyarfas, B.; Manna, S.; Biswas, S.; Borges, C.; Lindsay, S. *Nat. Nanotechnol.* **2014**, *9*, 466−473.
(34) Bui, P. T.; Nishino, T. *Phys. Chem. Chem. Phys.* **2014**, *16*, 5490−5494.
(35) Jeffrey, G. A. An introduction to hydrogen bonding. In *Topics in Physical Chemistry*, 1st ed.; Oxford University Press: New York, 1997.

Supporting Information

Highly Conductive Single-Molecule Wires with Controlled Orientation by Coordination of Metalloporphyrins

Albert C. Aragonès,[a,b] Nadim Darwish,[a] Wojciech J. Saletra,[c] Lluïsa Pérez-García,[d,e] Fausto Sanz,[a,b] Josep Puigmartí-Luis,[c,f,*] David B. Amabilino[c,*] and Ismael Díez-Pérez[a,*]

[a] *Departament de Química Física, Universitat de Barcelona, Diagonal 645, 08028 Barcelona, Spain and Institut de Bioenginyeria de Catalunya (IBEC) Baldiri Reixac 15-21, 08028 Barcelona, Catalonia, Spain*

[b] *Centro Investigación Biomédica en Red (CIBER-BBN). Campus Rio Ebro-Edificio I+D, Poeta Mariano Esquillor s/n, 50018 Zaragoza, Spain.*

[c] *Institut de Ciència de Materials de Barcelona (ICMAB-CSIC). Campus Universitari, 08193 Bellaterra, Catalonia, Spain.*

[d] *Facultat de Farmàcia, Universitat de Barcelona, 08028 Barcelona, Catalonia, Spain*

[e] *Institut de Nanociència i Nanotecnologia, Universitat de Barcelona, 08028 Barcelona, Catalonia, Spain.*

[f] *Empa, Laboratory for Protection and Physiology, Lerchenfeldstrasse 5, 9014 St. Gallen, Switzerland.*

*email: isma_diez@ub.edu, amabilino@icmab.es, josep.puigmarti@empa.ch

1. Pulling curves

Figure S1a shows 2D maps of hundreds of individual pulling traces collected during the break-junction experiment presented in Figure 1c of the manuscript for the DPP (left panel) and the Co-DPP (right panel). In order to investigate the correlation between the HC and MC/LC configurations, individual mechanical pulling curves of HC single-molecule bridge configurations were performed following a *blinking&pulling* scheme. An automatic algorithm in our program was set to detect a HC *blinking* event (such as the one in Fig. 3a, top trace) and immediately pull and record the corresponding pulling characteristic. Good correlation between the HC and the LC/MC events in the same trace is observed (Fig. S1b, red and black curves), which evidences the switching from the HC to the LC/MC configurations along the pulling of the molecular junction. In the absence of a single-molecule bridge, the pulling curves display an expected fast exponential decay with no plateaus (Fig. S1b, blue curve). In addition to this information, several of the latter control curves were averaged to get a tunneling decay constant of ~ 1.7 nm^{-1} in our working conditions. Considering a simple scenario of coherent electron tunneling through the gap (in the absence of a molecular bridge), we estimate a ~0.9 nm increase in the tip-to-substrate distance when going from a 9 nA to a 2 nA setpoint currents in Figures 3 an 4 of the main manuscript. This estimated distance is in good agreement with that obtained from the DFT optimized structures, which showed a tip-to-surface distance of 1.9-2.5 nm for the DPP configurations (see Fig. 5 and S6b) and 1.5 nm for the Co-DPP configuration (see Fig. 5).

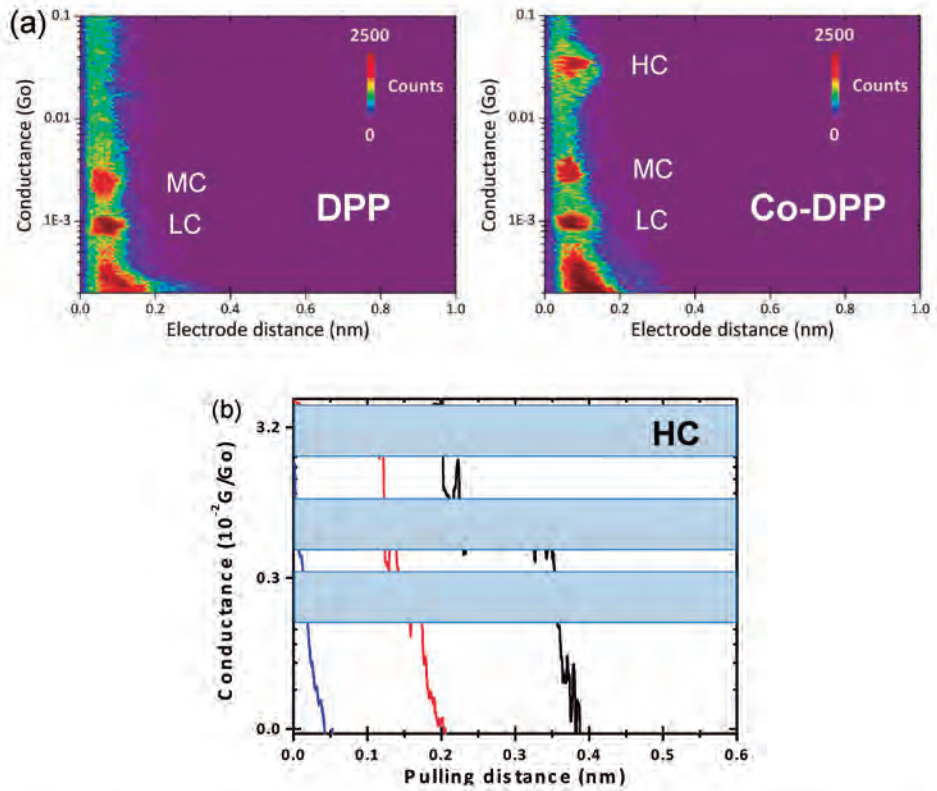

Figure S1. (a) 2D histograms from the break-junction experiments presented in Fig. 1c for DPP (left) and Co-DPP (right). A convenient color scale for counts has been set. (b) Representative induced STM tip pulling in the absence of a *blink* (blue) and after a HC *blink* is detected (red and black). Conductance ranges (HC, MC and LC) have been extracted from (a) and indicated in plot.

2. Average lifetime of the single-molecule junctions

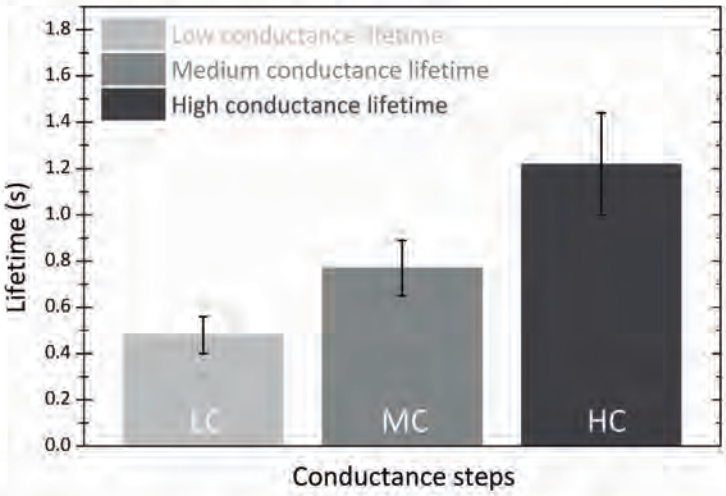

Figure S2. Average lifetime for the Low Conductance (LC), Medium Conductance (MC) and High Conductance (HC) *blinks* of the pyridinyl-coordinated Co-DPP junction at intermediate tip-to-sample distance (4 nA setpoint current).

3. Control experiments with pyridinyl-functionalized electrodes

We have performed key control experiments by collecting *blinking* traces at different tip-to-sample distances to rule out possible interactions between pyridinyl blocks from both electrode surfaces that could result in the formation of molecular wires (Fig. S3a). Inset S3a shows also a *soft* break-junction experiment (see experimental details in section 9) in the absence of porphyrins, displaying no clear peaks. Similar tip and surface functionalization has been recently exploited in molecular recognition experiments in an STM configuration[1]. Figure S3b shows the total 2D map combining all current traces (at the three tip-to-surface distances) normalized to a zero baseline. The total absence of bands in the 2D map, as opposed to the maps in the presence of porphyrins (Figs. 3b-c and 4a-c of the main manuscript), demonstrates the absence of interactions between the pyridinyl blocks from both electrode surfaces.

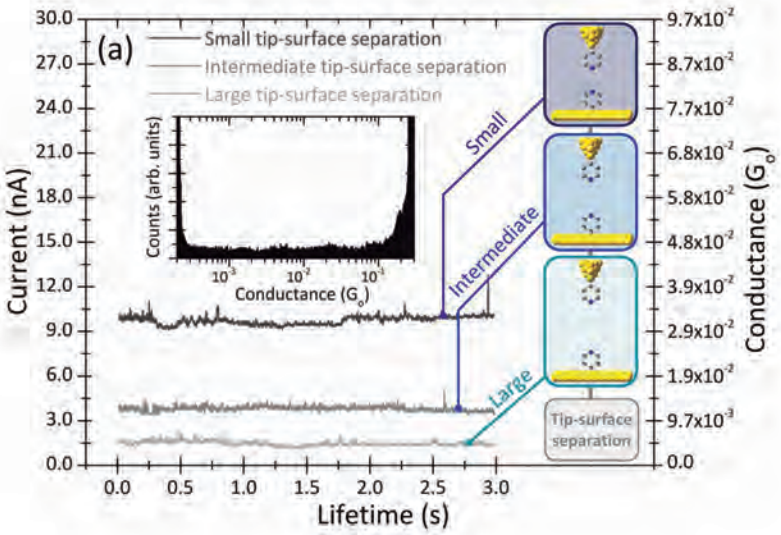

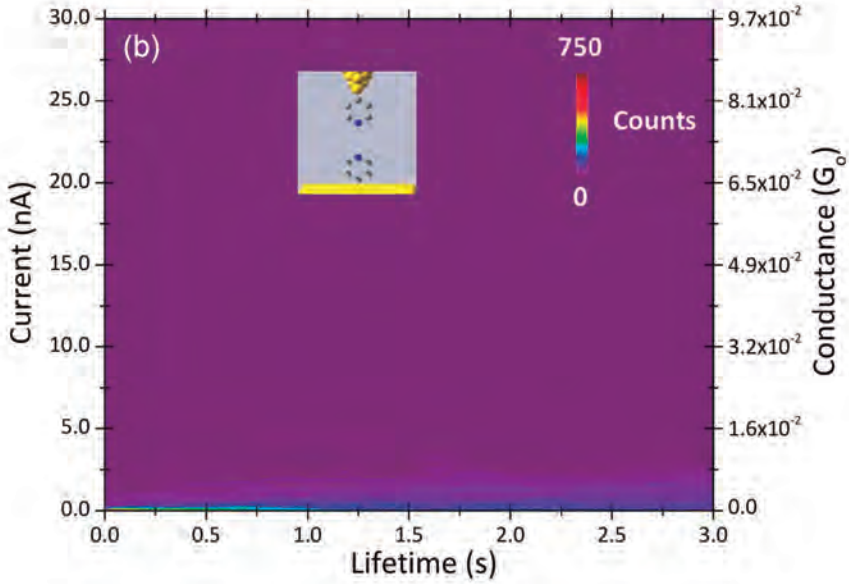

Figure S3. *Blinking* experiments in absence of the Co-DPP molecule with both tip and surface functionalized with pyridinyl groups at three different tip-to-surface gaps defined by 2, 4 and 9 nA setpoint currents for large, intermediate and small separations respectively. (a) Individual current captures. The inset shows a conductance histogram from a break-junction experiment in the absence of porphyrin (control experiment of Fig. 1c in the main manuscript). (b) The 2D *blinking* map combining all individual traces at the three different tip-to-surface gaps. All traces were set into a common time origin and a zero baseline.

4. Control *Blinking* experiments with non-functionalized tip and surface electrodes

We have performed additional control experiments by approaching the two bare electrodes (without pyridinyl functionalization) in the presence of porphyrins. The absence of any band in the 2D *blinking* map, as compare to the maps in Figs. 3b-c and 4a-c of the main manuscript, evidences the lack of any molecular wire formation in such junction configuration at the employed tip-to-sample working distances (Fig. S4).

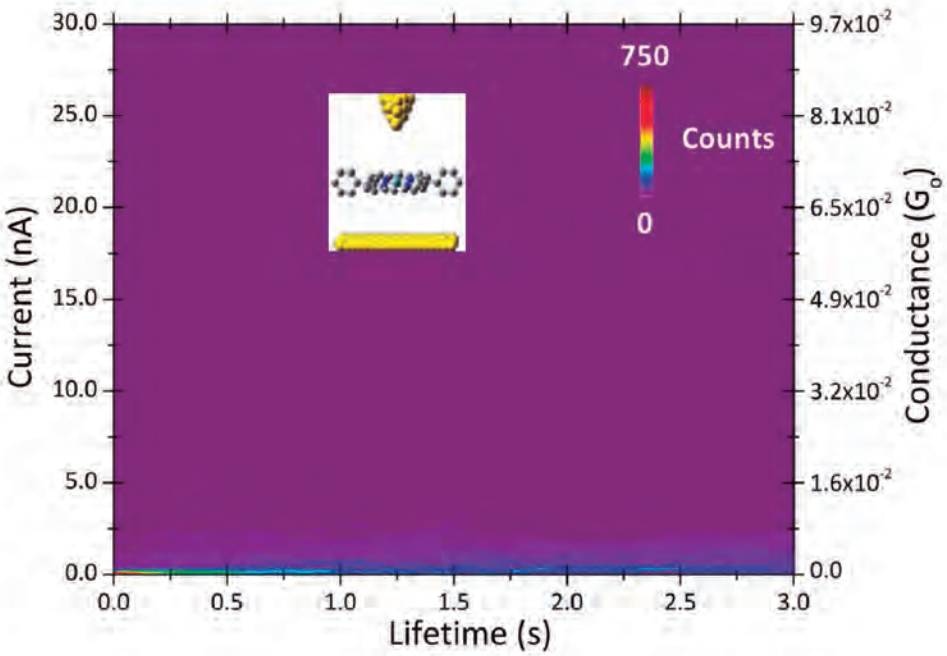

Figure S4. 2D *blinking* map in the absence of the pyridinyl units at the tip and substrate electrodes surfaces when porphyrin is present in solution. All samples were set into a common time origin and baseline.

5. *Blinking* 1D histograms at the three different setpoint currents

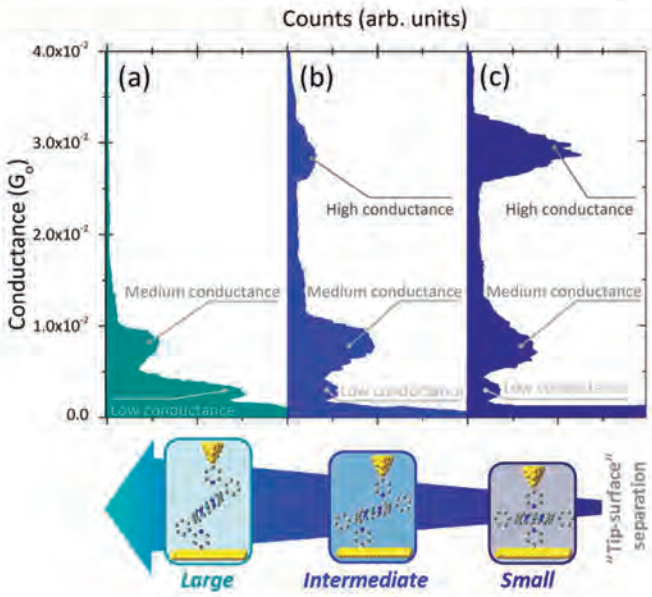

Figure S5. Conductance histograms obtained from *blinking* experiments of the pyridinyl-coordinated Co-DPP junction at the three different tip-to-substrate separations: (a) large, (b) intermediate and (c) small separation. See the estimated distances for (a) to (c) in section 1.

6. Normalization procedure

To normalize the variations of the total amount of counts among different experiments, normalized peak areas were calculated from the peak area of each individual peak in the 1D *blinking* histogram divided by the sum of the areas of all peaks.

$$Normalized\ peak\ area = \frac{peak\ area\ (individual)}{total\ areas\ (all\ peaks)}$$

7. Pyridine–DPP–pyridine H-bonding configurations

The geometry optimizations and calculated frontier orbitals were performed using Density Functional methods (DFT) within the B3LYP approximation. In order to consider heavy metal atoms, effective core potentials (ECPs) including relativistic effects were accounted by using a LANL2DZ basis set.[2] Figure S6a shows the optimization of the diphenylporphyrin ring and the corresponding frontier orbitals representation[3]. The high dihedral angle between the phenyls and the porphyrin ring (~81°) results in an electronic decoupling of the formers[4], *i.e.* poor electronic contribution of the phenyl groups to the molecular orbitals involved in the transport process. Hence, the phenyl rings have been removed from the junction geometry optimizations for simplicity.

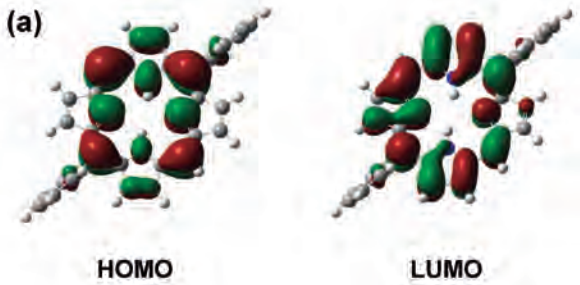

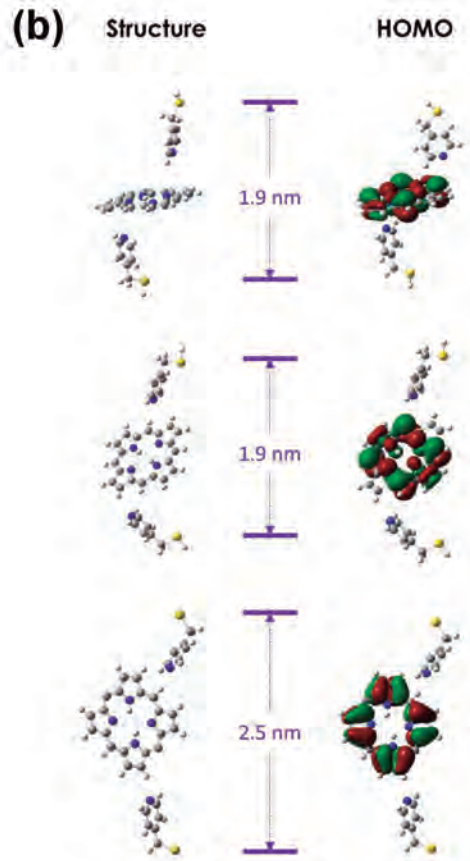

Figure S6. (a) Optimized geometry and molecular frontier orbital representations of the DPP block. (b) Optimized geometries (omitting diphenyl groups) alongside with the HOMO frontier orbital of the pyridine–DPP–pyridine H-bonding configurations.

8. Sample preparation

Pyridin-4-yl-methanethiol was synthesized as described previously by Puigmarti-Luis *et. al.*[5] DPP was purchased from Sigma-Aldrich and was used as received, and Co-DPP was synthesized according to the published procedure described by Song *et. al.*[6] and purified by column chromatography and crystallization. All glassware and Teflon STM cells were cleaned with piranha solution (1:1 H_2SO_4/H_2O_2 by volume) before usage

followed by rinsing with 18 MΩ cm^{-1} Milli-Q water (Millipore). An Au (111) single crystal substrate (10 mm x1 mm) of 99.9999% purity and orientation accuracy < 0.1 degrees was purchased from MaTeck (Germany). Before each experiment, the single crystal Au (111) substrate was electropolished to eliminate possible residual contamination and then annealed with a H_2 flame. The surfaces were then washed with argon-purged ethanol and dried under a stream of argon after which they were placed in 0.8-1 mM ethanol solution of pyridin-4-yl-methanethiol for 24 h. Au tips were mechanically cut, briefly H-flame annealed and immediately immersed in 0.8-1 mM ethanol solution of pyridin-4-yl-methanethiol for 24 h. The Au (111) surfaces and Au tips were then washed thoroughly with ethanol and dried under a stream of argon. The Au (111) surface was then assembled in the STM cell and the surface electrode filled with a 80 μL of pure mesitylene, where STM junction control experiments were firstly run. Next, few drops of a 8-12 nM mesitylene solution of the porphyrin was added to build the porphyrin mediated molecular wires.

9. Additional technical details of the single-molecule transport measurements

Single-Molecule Junctions. Details about the STM-break junction technique are published elsewhere.[7] All experiments were carried out with a homemade Teflon STM cell and a PicoSPM I microscope head controlled using a Picoscan 2500 electronics, all from Agilent. The STM head was mechanically and electronically isolated. Data was acquired using a NI-DAQmx/BNC-2110 National Instruments (LabVIEW data acquisition System) and analyzed with LabVIEW code. In a typical break-junction experiment, the STM tip is first brought to tunneling distance over a flat clean Au (111) surface area. The STM feedback is then turned off and the tip is driven into and out of contact with the substrate at 3 V/s. These 2-points feedback loop is used to collect

thousands of current decays (3000-4500) during the tip pulling cycles[1]. In order to minimize disruption of the tip and sample surface functionalization, the attained maximum current in the 2-points feedback loop was set to a low value well below saturation, which prevented the STM tip crashing against the substrate electrode. 15-20% of the collected current decays display steps (*plateaus*), and are used to determine the single molecule conductance using the expression $G=I_{step}/U_{bias}$ where G is the conductance, I is the current and U is the potential difference between the two junction electrodes. The current decays are accumulated to form linear and semi-logarithmic conductance histograms. The observed peaks in the conductance histograms correspond to the observed plateaus in the current decays and provide averaged single-molecule conductance values. An automated selection process designed by LabVIEW code was used to select the decays that showed plateaus from the ones that did not. The user defines the initial selection criteria that are fixed throughout all the experimental series. The yield of the decay curves showing plateaus was typically between 15 and 20% of the total collected curves. The bias voltage between the tip and substrate electrodes was set to 5 mV for all experiments.

The *blinking* captures (350-400 curves) were accumulated into 1D conductance histograms and 2D maps. No selection procedures were applied at this time and so all *blinking* traces are used to build the histograms. In order to compare the lifetimes of the blinks in the 2D maps, all the samples were set into a common time origin and baseline. The final STM tip pulling after the *blinking* was performed by externally controlling the piezo z-position. The current setpoint used (from 2 to 9 nA) for each capture has been indicated at the corresponding figure in the manuscript. The bias voltage between the tip and substrate electrodes was set to 5 mV for all experiments.

With the exception of Fig. S4, all experiments were conducted with mercaptopyridinyl-functionalized tip and surface electrodes.

References

1. Zhao, Y.; Ashcroft, B.; Zhang, P.; Liu, H.; Sen, S.; Song, W.; Im, J.; Gyarfas, B.; Manna, S.; Biswas, S.; Borges, C.; Lindsay, S. *Nat. Nanotech.* **2014**, *9*, 466–473.

2. Koch, W.; Holthausen, M. C. *A Chemist's Guide to Density Functional Theory. Neural Networks;* Wiley-VCH Verlag GmbH, Weinheim, Germany, 2001; Vol. *3*, p294.

3. Foresman, J.B. *Exploring Chemistry with Electronics Structure Methods;* Eleen Frisch, Gaussian Inc., Pittsburgh, PA, 1996; second Edition, p112.

4. Venkataraman, L; Klare, J.E.; Nuckolls, C.; Hybertsen, M.S.; Steigerwald, M.L. *Nature* **2006**, *442*, 904-907.

5. Puigmartí-Luis, J., Saletra, W. J., González, A., Amabilino, D. B.; Pérez-García, L. *Chem. Commun.* **2014**, *50*, 82–84.

6. Song, X. Z.; Jaquinod, L.; Jentzen, W.; Nurco, D. J.; Jia, S. L.; Khoury, R. G.; Ma, J. G.; Medforth, C. J.; Smith, K. M.; Shelnutt, J. A. *Inorg. Chem.* **1998**, *37*, 2009–2019.

7. Xu, B.; Tao, N. J. *Science* **2003,** *301*, 1221–1223.

3.1.3 Findings and Discussion

— The main findings of this study were the following:

- *Tapping* experiments for the Co-DPP show three distinguishable different current signatures at the conductance ranges of ca. $3x10^{-3}G_o$ (LC), $8x10^{-3}G_o$ (MC) and $3x10^{-2}G_o$ (HC). DPP shows the two same low conductance peaks of ca. $3x10^{-3}G_o$ (LC) and $9x10^{-3}G_o$ (MC).

- The trend of the blinks lifetime follows a close parallelism to the presented by the conductance, the longest lifetime is showed for the HC, followed by MC and the LC, being the latter slightly shorter.

- *Blinking* experiments for the Co-DPP and DPP molecules show the same current signatures obtained by employing the *tapping* approach. Each of the three current signatures associated to the Co-DPP, changes its *blinking events* frequency according to the tip-surface gap distance with the following trend: The HC signature is inexistent under large electrodes separation and increases with the electrode proximity, contrary the LC case shows the opposite trend, is the most probable current signature under a large electrodes separation and decreases (but no disappears) with such separation, MC is the most stable current signature despite the slightly increment at intermediate electrodes separations.

- Pulling curves collected during the selected *blinking* events showed plateaus before the sharp current decay. Contrary, the exerted on the tunneling current showed a sharp exponential current decay immediately after the application.

- *Blinking* experiments performed in the absence of Co-DPP or DPP molecules, with both Ni tip and substrate electrodes *Pyr*-functionalized as well as in the absence of the *Pyr* units at the Ni tip and substrate electrodes but Cu-DPP molecules present in solution, none of the two controls experiments did show any current signal.

- The optimized structure for the hexacoordinated *Pyr*–Co-DPP–*Pyr* adduct shows Co–N distances of less than 2 $\mathring{A}$ and a flat conformation. The HOMO orbitals are extended along the junction main axis between both N-*Pyr* N-*Pyr* units and also localized over the *porphyrin ring*. The optimization results for the *Pyr*–DPP–*Pyr* adduct show multiple relaxed conformations with the *porphyrin ring* highly tilted and interacting with the two N-*Pyr* groups. The HOMO and LUMO frontier orbitals of such conformations are mainly localized on the DPP *porphyrin ring* close to the obtained from the isolated DPP molecule.

— The discussion of the results is summarized below:

- The presence of the HC signature is observed on *tapping* and *blinking* measurements for the Co-DPP molecule, but contrary, it is absent in the analogous DPP measurements, therefore it proves that such HC signature depends straightly on Co center. This strongly suggests that HC corresponds to the aimed junction of the hexacoordinated Co via the axial binding through the two N-*Pyr* provided by each functionalized electrode. Idea asserted by the high population of the HC *blinking* events detected using small electrodes separations, from which can be extracted that such small tip-surface gap distances stabilize the flat conformation, very feasible scenario since Co hexacoordination via the *Pyr* units requires the Co-DPP molecule to be oriented flat at the junction with short Co–N-*Pyr* distances.[479–481]

- The proposed scenario extracted from the current measurements is supported by the obtained optimization structure for the *Pyr*–Co-DPP–*Pyr* adduct, a flat conformation of the hexacoordinate Co with a significant small Co–N bonding distances of less than 2 $\mathring{A}$, values consistent with the obtained from the resolved X-ray crystal structures of hexacoordinated *Pyr*–Co metalloporphyrin–*Pyr* axially linked.[479]

- The LC and MC signatures observed on *tapping* and *blinking* measurements, are common for both DPP and Co-DPP molecules, but their presence on the former molecule imply that the associated junction only can be formed via *porphyrin ring*–N-*Pyr* interaction due the metal absence, thus is assumed an interaction via H-bonding. Since the multiple available active bonding sites of the *porphyrin ring*, such H-bonding with the N-*Pyr* can be established through various of those active sites, justifying the existence of different conformations distinguishable by current signals like the observed LC and MC signatures.

- The predominant presence of the LC and MC signatures at intermediate and large electrodes separations implies the presence of H-bonding at those large distances, but it does not, however, can exclude such "weak" interactions like recent experimental works attest wiring two electrodes through such interactions.[482,483] This scenario is also supported by the calculated geometries of *Pyr*-DPP-*Pyr* adducts under large and intermediate electrodes separations. The obtained geometry optimizations show conformations stabilized by long-distance interactions between N-*Pyr* units and different active sites of the *porphyrin ring* via the H-bonding. Some of such conformations are highly tilted like in larger S-to-S junctions, scenario qualitatively analogous to the experimental results, justifying the overwhelming presence of the MC and LC signature at large and intermediate electrodes separation.

- The average lifetime of the HC blinks is ca. 1.5 seconds at small tip-surface gap distances, which suggests that the hexacoordinated (planar) junction associated to the HC blinks are significantly more stable than the analogous

MC and LC. The observed junction lifetime for each conductance signature is comparable between the three tip-surface distance cases, excepting the slight increment of ca. 0.25 s of lifetime showed by the HC case, when it goes from intermediate to small tip-surface distances. This suggests a partially strained Co-DPP junction in the case of intermediate distances thus resulting in a premature mechanically induced junction collapse decreasing the overall complex stability. The higher stabilization (high binding energy) for the Co–N-*Pyr* also is confirmed since avoids any optimized conformation for Co-DPP molecules other than that implies Co hexacoordination.

- The HC signature attributed to the hexacoordinated *Pyr*–Co-DPP–*Pyr* is justified by the delocalization of calculated orbitals on the extended electronic-pathway along the junction main axis between the two electrodes. However, the suppression of HC level in the DPP junctions due the absence of the metal center and the resulting lack of delocalized orbitals along junction main axis, shows a scenario very close to the obtained from the isolated DPP molecule justifying the unfavored electron-pathway. It affects straightly to the measured conductance of the single molecular wire, as is observed on the junctions done by DPP but also present for the Co-DPP case established jointly with the HC signature. The inherent characteristics between the two different electron-pathways associated to HC or the MC and LC, justifies the observed conductance difference for both between a factor 5 and one order of magnitude.

- Tapping approach did not biased the results, although is not able to explain the different conductance ranges since it cannot fix a electrodes separation.

- Pulling curves collected during the selected *blinking* events showed plateaus. Contrary, the exerted on the tunneling current showed a sharp exponential current decay immediately after the application.

3.2 Spin-dependent transport in Metalloporphyrins

In the prior section was developed a new method to build single-molecule wires based on a flat metalloporphyrin conformation via the axial coordination of the central metal center. Through measuring the Co-DPP conductance, were studied the binding sites of electrode-molecule and the effects over the conductance as well as their dependence to tip-substrate electrodes distance. The aim of this section is introducing the learned Spintronics concepts of the preceding chapter to develop a spin-filtering single-molecule device exploiting metalloporphyrins.

The unique experimental referent of spin-dependent transport involving metalloporphyrin was reported by Schamus and coworkers on 2011,[318] employing a LT-STM and obtaining a MR efficiency of 60%. In such work, the conductance of a polarized current was tuned depending a Co nano-island's magnetic moment parallel or antiparallel to a used STM Tip's magnetic moment direction. The reported mechanism is based in the TMR effect (see *Section "Tunneling Magnetoresistance"*, on Page 41) and differs drastically from the presented model on the preceding chapter. This is because in the reported experiments, the observed TMR was the direct consequence of the interplay between two electrodes, the Co-islands (with a fixed spin direction) and the STM tip (with a variable spin-direction), thus the molecule does not present any significant role to the TMR mechanism because was merely the linker between both electrodes. Furthermore, LT conditions were required to keep the Co nano-island's magnetic moment direction, differing from the scenario obtained at RT using an enough strong Spinterface effect causing the polarization of the current, like the observed in the preceding chapter.

Several theoretical studies analyzed the metalloporphyrin's spin-filter capabilities,[191,300,391–393] and perceived these molecules as the ideal candidates to build a single-molecule device with spin-dependent current response.[191,391–394] Such works studied different metalloporphyrins with different open-shell metal centers such as Fe,[392,394] Co,[300,391,484] Cu,[300] Mn[191] or Cr.[393] This paramagnetic electronic configuration is the fundamental requirement[298,300] to present different affinities to the electron spin-polarizations. From the previous results can be extracted that open-shell metalloporphyrins have the proper asymmetric electronic structure to show significant distribution differences by the spin-polarized states (see Figure 3.6),[191] which form efficient spin-selective channels[191,391,392,484]) with occupied or empty orbitals[391,393] close to the ε_F of the junction electrodes. As a consequence, the efficiency of the electronic transport depends on the spin-polarization, as reveal the calculated DOS[393] and T(f)[300,392,484] curves. Also is exposed that the metal coordination can affect to the spin-filtering properties, like the case of Fe metalloporphyrins,[392] which present higher energy differences between spin-polarizations given the axial coordination of the metal center,[392] likewise the presented on this chapter in order to achieve the planar conformation. Another essential property is the capacity of the metalloporphyrins' magnetic moment direction to be aligned according to a polarized electrode, scenario extensively studied for Cr metalloporphyrins.[393] In such molecules, the energy involved in the flipping of the molecular

spin is ca. 5 K, therefore at RT conditions any MA effect is suppressed and the molecule's spin can be readily oriented according to magnetized electrodes,[393,394] similarly to the observed on the previous chapter with the metal complexes and the Ni tip, thus used in the current chapter too.

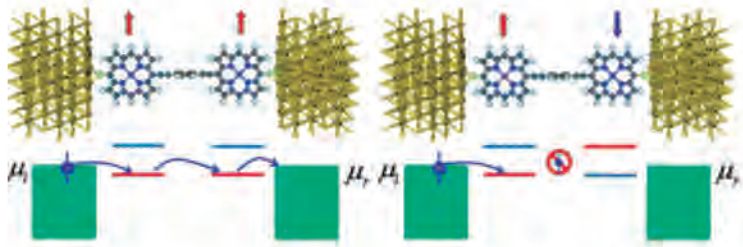

Figure 3.6: Schematic representation of a proposed single-molecule spin-valve based on metalloporphyrins' spin-filtering capabilities to tuning the injected polarized-current. Depending on the parallel (left) or antiparallel (right) configuration the spin-transport is allowed or prevented, respectively. Adapted from Zeng et al.[191]

The main novelty presented on this study is the employment of a Ni tip magnetic polarization direction perpendicularly to the electron-pathway. This is not a completely new concept, in fact is an old effect discovered by Sir William Thomson (Lord Kelvin) in 1857,[485] called AMR (Anisotropic magnetoresistance) which has been extensively explored but on the bulk scale and especially on ferromagnets.[486,487] This effect over the conductance depends on the orientation of the magnetization (MR) respect to the electric current direction in a material and can happen on both CPP or CIP geometries. Many decades later and applied to the nanoscale, this effect was tested in nano-contacts where the ballistic conductance was tuned according to the direction of an applied EMF respect an injected current.[488,489] Also, this effect has been applied using multi-layered sandwiched metallic systems under tunneling regimes,[490–492] known as TAMR (Tunneling Anisotropic Magnetoresistance) and very recently in single-molecule conductance experiments.[320] In the latter, were employed diamagnetic molecules used purely as linkers between polarized electrodes, thus did not represent a relevant role on the detected spin-dependent transport. In this section, this new perpendicular polarization direction complements to the already used in the previous chapter to study the spin-dependent transport on metalloporphyrins. The novelty of the proposed study using the AMR effect, is the employment of paramagnetic molecules aiming to enhance the filtering capabilities of the molecules thanks the associated the SOC as theoretical works proposed due the crucial role of the molecule.[487]

As has been described, metalloporphyrins are great candidates to design molecular-junctions with spin-selective transport. Their theoretically predicted features fit with the requirements of the proposed model developed in the preceding chapter, therefore they will be employed as the central elements for the presented single-molecule device. Since metalloporphyrins are open-shell molecules, it represents their fundamental property to be used as the *first key-parameter* like the previous metal complexes cases. Because of these electronic configuration, metalloporphyrins

can provide the asymmetry to the system due their spin-carriers' preferences as well as their magnetic moment can be aligned due the inherent paramagnetism. It will happen according the Ni tip electrode magnetization direction (*second key-parameter*), arising the desirable "switching" behavior to the junction, mirroring the observed "current tuning" effect employed on metal complexes. Finally, the Spinterface will be also present as the third *key-parameter* in this single-molecule device, with the aim to pre-polarize the injected current to the metalloporphyrin.

The expected phenomenology is the observed in the prior chapter. Mainly, will be performed conductance measurements of asymmetric junctions where the current will be polarized at the Au-surface Spinterface and then injected to the metalloporphyrin; according to the Ni tip polarization direction, the metalloporphyrin magnetic moment will be oriented, and depending it, the measured current through the junction will be tuned. Once more, the most accurate way to combine the three *key-parameters* is employing the STM at RT to conduct single-molecule current experiments, aiming to study the spin-dependent transport through the junction.

3.2.1 The experimental research

In this section is explained how a new single-molecule spin-filter device was developed at RT employing a *set-up* based on an STM microscope and using the novel metalloporphyrin junctions via axial coordination. In these experiments the employed molecules were: Co(II)-5,15-diphenylporphyrin (Co-DPP), the Ni(II)-5,15-diphenylporphyrin (Ni-DPP), the Cu(II)-5,15-diphenylporphyrin (Cu-DPP) and the Zn(II)-5,15-diphenylporphyrin (Zn-DPP), synthesized according to the procedure described by Song et al.[476,477] To study the effects of spin-dependent electron transport were gathered three ingredients associated to the explained asymmetric *key-parameters* in the preceding chapter, which are: the ***open-shell/paramagnetism*** with spin-dependent transport channels, the Ni tip ***magnetic polarizations*** and the ***Spinterface***. In this occasion, the former *key-parameter* was incorporated via the first *ingredient*through three possible metalloporphyrins (*i*): The already studied Co-DPP molecule under non-polarized electrodes, the Ni-DPP or Cu-DPP; the Zn-DPP was used as a control due its *closed-shell* electronic structure. Similarly to the procedure previously used, the second *ingredient* was once more introduced via a ferromagnetic Ni STM (*ii*) *ex-situ* magnetized in α-$\uparrow$Ni or β-$\downarrow$Ni magnetic polarizations as well using the *perpendicular* magnetic polarization direction, all of them aimed to tune the spin-dependent transport. The third *ingredient* was the Au(111) substrate electrode (*iii*), because the polarization effect through the Spinterface was fundamental. Regarding the Spinterface, the proposed device also contains its two proved requirements: the a essential S-Au strong polarizing effect, achieved thanks to the "*Pyr*" (functionalization) molecules since contain -SH as anchoring group, as well as the critical molecular paramagnetism used to enhance the Spinterface effect, achieved thanks to the open-shell used metalloporphyrins (first ingredient). All the three *ingredients* analogous to the *key-parameters* and the proposed model are summarized in Figure 3.7.

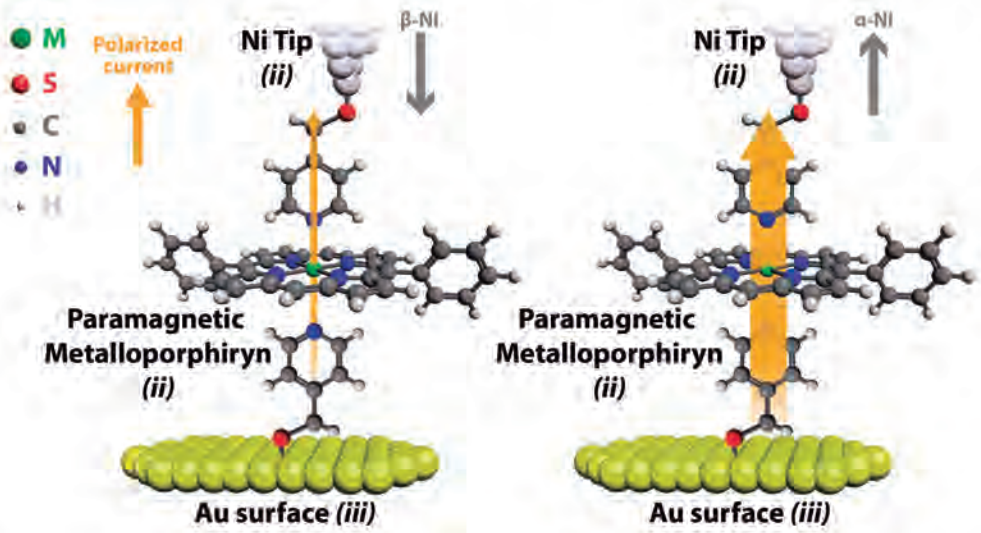

Figure 3.7: Schematic representation of the single-molecule device based on metalloporphyrins showing spin-filtering capabilities with the three "ingredients" labeled.

The STM experiments were carried out employing polycrystalline Ni wire to obtain the STM tips electrodes as well as Au(111) monocrystals were utilized as substrate electrodes, the used medium was mesitylene organic solvent. The employed procedure was the STM-BJ (see *Section "STM Break-Junction Technique"*, on Page 26) into its two common approaches, the dynamic *tapping* and the static *blinking* (see *Appendix C.1*, Page 325) with different objectives. The former approach, like in previous occasions, was used in order to obtain thousands of current decays from the established junctions allowing to perform a robust statistical analysis of the different experimental conditions to study the effects of the Ni tip polarization on the measured current. The latter approach was used to obtain similar spin-dependent current measurements but also avoiding any kind of stretching-dependent conductance effects, potentially presented by *tapping* approach, aiming to attest the observed MR phenomena as the uniquely consequence of the Ni-tip polarization. For this reason and according to the obtained results of the previous section, the tip-surface gap fixed distance was established to a set-point current of 7 nA, distance associated to a small electrodes separation which favors the axial metal coordination. Since the main drawback of the*blinking* approach is its lack on statistics, both techniques should be employed since they are mutually complementary. A detailed description of the electrodes preparation and functionalization, the Ni tip polarization as well as the molecular adsorption procedures, can be found from Page 328 (*Appendix C.2*).

The performed measurements were supported by periodic DFT computational calculations using *Siesta-Gollum PBE+U*, aiming to corroborate the current spin-dependence focusing on the existence of the α or β channels defined by the electronic structure of the paramagnetic molecules and their mixing with the Au surface levels through DOS and T(f) curves. Geometries were optimized using Gaussian09/ *TPSSh* to provide a better estimation of the state energies of transition metals complexes.

3.2.2 Objectives and Summary of the experimental work

- The dynamic STM-BJ *tapping* approach was used to perform thousands of junctions to study the spin-dependent current response on the established singe-molecule device for the Co-DPP, Ni-DPP and Cu-DPP metalloporphyrins, the experiments were done employing α-$\uparrow$Ni and β-$\downarrow$Ni polarizations and a bias voltage between the -7.5 mV *Au substrate-to-Ni tip* current sense.

- In order to assess the effect of the current sense over the spin-dependent transport were inverted the electrodes source and drain roles. Single-current measurements employing the *tapping* approach were conducted under the *Ni tip-to-Au substrate* current sense applying a bias voltage of +7.5 mV employing α-$\uparrow$Ni and β-$\downarrow$Ni polarizations.

- To evaluate the effects of the magnetized electrode were used a Au substrate and non-magnetized Ni tip electrodes to conduct single-current measurements for Co-DPP, Ni-DPP and Cu-DPP metalloporphyrins at both current senses ($\pm$7.5 mV).

- To study the effects over spin-dependent transport of the paramagnetic state of the metalloporphyrins, were performed junctions with the diamagnetic Zn-DPP (S=0) as a control under all the previous experimental and also employing the *tapping* approach.

- *Tapping* experiments were performed in the absence of the *Pyr* units at the Ni tip but with functionalized substrate electrode to study the possible pentacoordination of the metalloporphyrins.

- *Blinking* experiments were done employing a non-magnetized Ni tip and a Au substrate, aiming to attest the origin of the multiple conductance peaks to the contact geometries like in the break-junction experiments of the previous section, where were employed Au Tip and substrate electrodes. Were used a bias voltage of the -7.5 mV *Au substrate-to-Ni tip* current sense and initial set-point current of 7 nA.

- The *blinking* approach was used to study the spin-dependent current response of Cu-DPP, the experiments were done employing α-$\uparrow$Ni, β-$\downarrow$Ni and $\perp$Ni polarizations under a bias voltage of the -7.5 mV *Au substrate-to-Ni tip* current sense and initial set-point current of 7 nA. The objective of these sets of experiments were the validation of any spin-dependent effect exclusively to the Ni tip polarization, preventing any mechanical effect since to the approach stability.

- To ascertain unequivocally the establishment of a molecular junction between the two electrodes during the *blinking* experiments, like in previous occasions mechanical pullings over a *blinking* event were applied. Besides, as a reference of a junction-free scenario also was applied the same procedure under current

tunneling through the gap. For a more detailed description of this procedure see *Appendix C.1* (Page 325).

- To assigns the low observed conductance signatures observed in the previous Section and present to the current, different control experiments were performed employing tetra-phenilated DPPs and phenilated-free DPPs.

- *Tapping* and *blinking* experiments were performed in the absence of metalloporphyrin molecules with both Ni tip and substrate functionalized with *Pyr* groups and also in the absence of the *Pyr* units at the Ni tip and substrate electrodes when Cu-DPP is present in solution, to confirm all the current signatures to the bonding between de metalloporphyrin and the N-*Pyr*.

In the following pages is shown summarized the research as an "under revision manuscript" and its Supplementary Information, excluding the .log files form computational results:

"Albert C. Aragonès, Alejandro Martín-Rodríguez, Fausto Sanz, Ismael Díez-Pérez and Eliseo Ruiz. Identifying spin-dependent electron-pathways in supramolecular metalloporphyrin wires. *Nature Chemistry, under revision*, 2017".

Identifying spin-dependent electron pathways in supramolecular metalloporphyrin wires

Albert C. Aragonès,[†,‡,§] Alejandro Martín-Rodríguez,[◊,‡] Arantzazu Gonzalez Campos,[⊥] Núria Aliaga-Alcalde,[⊥,¥] Daniel Aravena,[#] Fausto Sanz,[†,§], Eliseo Ruiz,[◊,‡*] Ismael Díez-Pérez[†,‡,§*]

[†] Departament de Ciència de Materials i Química Física, Universitat de Barcelona, Martí i Franquès 1 and Institut de Bioenginyeria de Catalunya (IBEC) Baldiri Reixac 15-21, Barcelona 08028 Spain

[‡]Institut de Química Teòrica i Computacional, Universitat de Barcelona, Diagonal 645, 08028 Barcelona, Spain

[§] Centro Investigación Biomédica en Red (CIBER-BBN). Campus Río Ebro-Edificio I+D, Poeta Mariano Esquillor s/n, 50018 Zaragoza, Spain.

[◊] Departament de Química Inorgànica i Orgànica, Diagonal 645, 08028 Barcelona, Spain

[⊥] CSIC-ICMAB (Institut de Ciència dels Materials de Barcelona) Campus de la Universitat Autònoma de Barcelona, 08193 Bellaterra, Spain.

[¥] ICREA (Institució Catalana de Recerca i Estudis Avançats)

[#] Departamento de Química de los Materiales, Facultad de Química y Biología, Universidad de Santiago de Chile (USACH), Casilla 40, Correo 33, Chile

ABSTRACT

Spin-dependent effects in single-molecule junctions based on metalloporphyrin molecules shown non-precedent effects: the largest conductance value reported for a molecular-based magnetoresistance single-junction also the Co^{II} and Cu^{II} systems are the first examples of existence of magnetoresistance effect either injecting, as usual, the electrons from the gold substrate or from the magnetically-polarized nickel tip. Furthermore, the application of a perpendicular magnetization to the nickel tip also show a non-previously described effect suppressing the transport channels with contribution of the magnetic metal cations. Thus, such single-molecule junctions present a large anisotropy on the magnetoresistance effect depending the orientation of the magnetization of the magnetic nickel tip. DFT calculations show the key ingredients in the electronic structure of the magnetic molecules as well as the spinterface created with the electrodes, as main feature the transport through the single-molecule junctions based on metalloporphyrin molecules is mediated by majority hole carriers.

Keywords: Single-Molecule Junctions, Metalloporphyrines, Magnetoresistance, Density Functional Calculations, Spinterface

Magnetoresistance is the crucial property for the development of spintronic devices. Usually, such property has been described in devices composed by multi-layered materials, usually a non-magnetic layer sandwiched between two magnetic metal electrodes. Molecular systems are an appealing alternative because they offer the opportunity to tune their physical properties, and in particular their magnetic properties, by introducing small changes in their structure. In this vein, magnetic molecular systems, such as the popular single-molecule magnets (*i.e.* Tb^{III}),[1–3] must be employed at cryogenic temperatures to preserve their intrinsic molecular magnetic properties, which severely limit their technological applications. Two different sets of molecular devices have been recently described showing room temperature spin-dependent transport: (i) chiral diamagnetic structures such as for instance DNA or peptide structures deposited on metal surfaces, display the well-described Chiral Induced Spin Selectivity (CISS) effect, reported by Naaman and coworkers.[4–7] The electron transport through one of the enantiomers shows a preference for one of spin carriers while the other enantiomer for those with the opposite spin.[8] (ii), Single-molecule junctions built by bridging individual small magnetic molecules such as high-spin transition metal complexes $[M(tzpy)_2(NCX)_2]$, (M: Fe or Co; X = S or Se) previously reported by us.[9,10] In this case, room-temperature magnetoresistance is observed when electrons are injected from the gold substrate to a magnetic nickel electrode through the transition metal complex that acts as spin filter. The inversion of the magnetization of the nickel electrode causes a huge change in the conductance value through the molecule. This effect is due to a subtle interplay in the electronic structure of the *spinterface* generated by the interaction of the magnetic molecule with the heavy Au metal substrate resulting in large spin-orbit effects.[11,12]

Here, we design and synthetize a series of metalloporphyrin complexes to build single-molecule contacts and characterize their spin-dependent charge transport using a spin-polarized version of the STM break-junction technique[13] using ferromagnetic STM probes.[9,8,10] The STM junction technique is used in two different working modes: the break-junction (STM-BJ) [13–15] and the spontaneous formation of molecular junctions.[16,17] In order to explore different electron pathways along the metalloporphyrin moiety,[18] we exploit our previously designed single-molecule supramolecular

platform where a metalloporphyrin is trapped in the tunnelling junction in at least two distinct conformations; perpendicular[19] (through-metal channel) and extended (through-ring channel).[9,10] Briefly, we chemically modify both STM Ni-tip and Au (111) surface electrodes with pyridin-4-yl-methanethiol (p4m) allowing the metalloporphyrins molecules dissolved in the solution to close the circuit through specific coordination of the metal and/or the ring with the pyridine (Figure 1). We studied four metalloporphyrin (M-DPP) with M^{II} (M : Co, Ni, Cu and Zn) cations and a non-metal porphyrin 5,15-diphenylporphyrin ligand (DPP). The results of this study show: (i) magnetoresistance effects in such molecular junctions at considerably larger conductance values than previously reported metal complexes. (ii) Only the transport channels through the metal cations are spin-dependent. (iii) Spin-dependent transport is not only limited to one bias sign (up to now magnetoresistance was only reported by injection from the gold substrate). (iv) The magnetization of the magnetic STM tip perpendicular to the transport direction blocks the spin-polarized electron transport through the metal transport channels and, consequently, shows a huge anisotropy in the magnetoresistance effect.

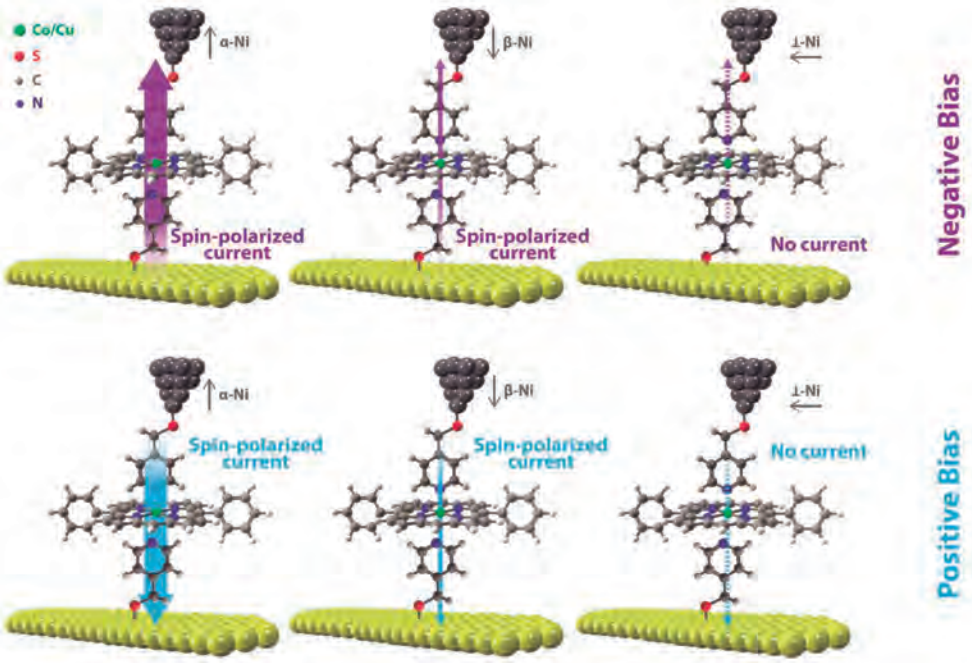

Figure 1 | Schematic representation of the studied Cu/Co-DPP flat configuration single-molecule junction under the three Ni tip magnetic polarizations (labelled in the figure as α-Ni, β-Ni and ⊥Ni) and the two bias. Among the four studied metalloporphyrin systems only Co^{II} and Cu^{II} systems show magnetoresistance. Such effect is larger when the electrons are injected from the gold substrate but also is present when electrons are injected since the Ni tip. Perpendicular Ni magnetic polarization blocks the electrons transport leading to a huge anisotropic magnetoresistance effect.

Results and discussion

Room-temperature single-molecule transport of the [M^{II}(DPP)] complexes (M = Co, Ni, Cu and Zn). Single-molecule conductance experiments were performed at room temperature using a spin-polarized version of the STM break-junction approach. Briefly, a freshly cut Ni tip was magnetically polarized *ex situ* by placing it in a few millimetres proximity to a permanent 1 T NdFeB magnet for a period of 2 h in an Ar controlled atmosphere chamber that preserves the tips from environmental oxidation.[9,8,10] After the magnetization, the Ni tip was placed into the STM tip holder. Then the STM current feedback was turned off and the polarized Ni tip was repeatedly driven in and out of contact to the Au(111) surface in successive cycles, using a 2-point feedback loop on the tunnelling current flowing between the two STM electrodes under a constant bias voltage.[13] During the retraction stage, individual molecules dissolved in the surrounding organic medium can spontaneous bridge between the two functionalized STM electrodes resulting in the collection of large amounts of current decay curves (4000–5000, see representative current captures in Supplementary Information section S1). Of these curves, 15-20% display plateau features corresponding to the quantum conductance of the single-molecule bridge.[9,20–23] The magnitude of the magnetic Ni tip polarization was characterized before and after the STM break-junction experiment using SQUID magnetometry to ensure that the Ni polarization persisted over the entire time frame of the experiments (see Supplementary Information section S3).[9,8,10]

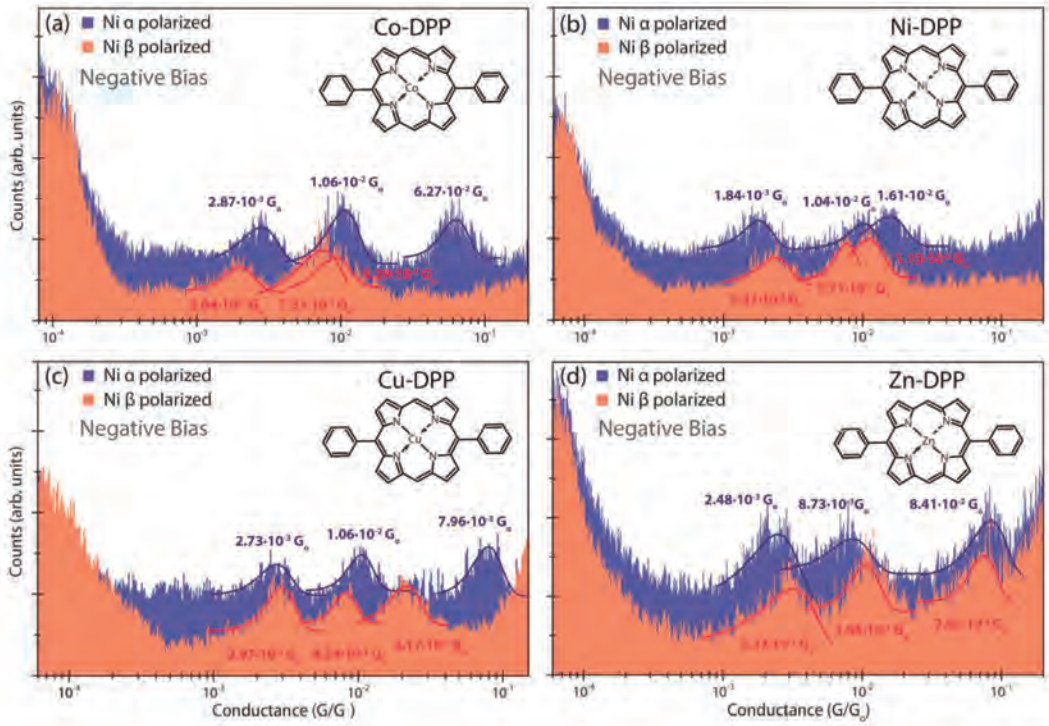

Figure 2 | Single-molecule conductance histograms injecting the electrons from the gold substrates. Schematic single-molecule conductance 1D log-histogram for the metal porphyrins (labelled and represented in the figure) bridging between Au and both α (blue) and β (orange) magnetically polarized Ni tips. Both histograms been vertically offset for clarity. All conductance values have been extracted from Gaussian fits of the peaks. The applied bias was set to −7.5 mV.

The results of the STM-BJ experiments are summarized in the histograms of Figures 2 and 3, which are built from hundreds of individual current decay captures (see Supplementary Information sections S1 and S4). In the conductance histograms of Figure 2 (injection of electrons from the gold substrate, negative bias), all four scenarios share two conductance regions, a low conductance (LC) region level in the range of 2-3 × 10^{-3} G_o and a medium conductance (MC) region in the range of 8×10^{-3} - $1x10^{-2}$ G_o, both related to the attachment of pyridinyl ligands with the backbone of the metalloporphyrin through hydrogen bond interactions as have been previously reported.[19] These assignments have been corroborated by performing the experiments with the tetraphenylporphyrin (without metal) showing only the LC and MC peaks.(see Supplementary Information section S1.4). For all studied metalloporphyrins, the highest conductance (HC) feature in the histogram is

univocally assigned to the metal complexation (perpendicular conformation),[19] and whose value varies from metal to metal [scientific report]. At a first glance, it is surprising the highest conductance value for the Zn^{II} system taking into account the closed d shell present in such metal cation. Hence, new experiments were performed by now using non-functionalized tip electrodes (see Supplementary Information section S1.5). These results reveal that no peak in the histograms are measured for the Co^{II}, Ni^{II} and Cu^{II} systems indicating that the non-functionalized tip cannot interact directly with such complexes, however, for the Zn^{II} complex a peak with a similar conductance to that found with the functionalized tip indicating that Zn^{II} cations both cases adopt an structure with coordination five [ZnDPP(p4m)]. It is well-know the tendency of such cation to present this coordination number and the presence of only one axial ligand will reduce the length of the transport channel in comparison with the other metal single-junctions justifying its largest conductance value.

Figure 2 shows that when the electrons are directed from the Au substrate to the polarized Ni tip, the LC and MC values show minimal variations under either α-Ni tip or β-Ni tip polarizations (poor magnetoresistance). In contrast, HC values display magnetoresistance with magnitudes depending upon the paramagnetic character of the metal complex. The [Co-DPP$(p4m)_2$] and [Cu-DPP$(p4m)_2$] complexes, both paramagnetic systems, show HC values significantly increasing under α-Ni tip and decreasing under β-Ni tip magnetizations. The difference between the HC values obtained under α-Ni tip and β-Ni tip polarizations directly depend on the metal core: 6-fold and 4-fold for the Co-DPP and Cu-DPP, respectively. It is worth remarking that such conductance values are the largest reported for molecular system showing magnetoresistance effects. Contrary, Ni-DPP and Zn-DPP molecules do not show significant conductance dependence upon magnetization of the Ni tip. The diamagnetism of the Zn-DPP complex explains the absence of magnetoresistance in this case. The Ni-DPP complex paramagnetism is very sensitive to the Ni coordination sphere, which inform us on the particular coordination[24–27] of the Ni-DPP in the junction that results in a low spin state (S=0) that yields poor magnetoresistance (further discussion will be given in the last section).

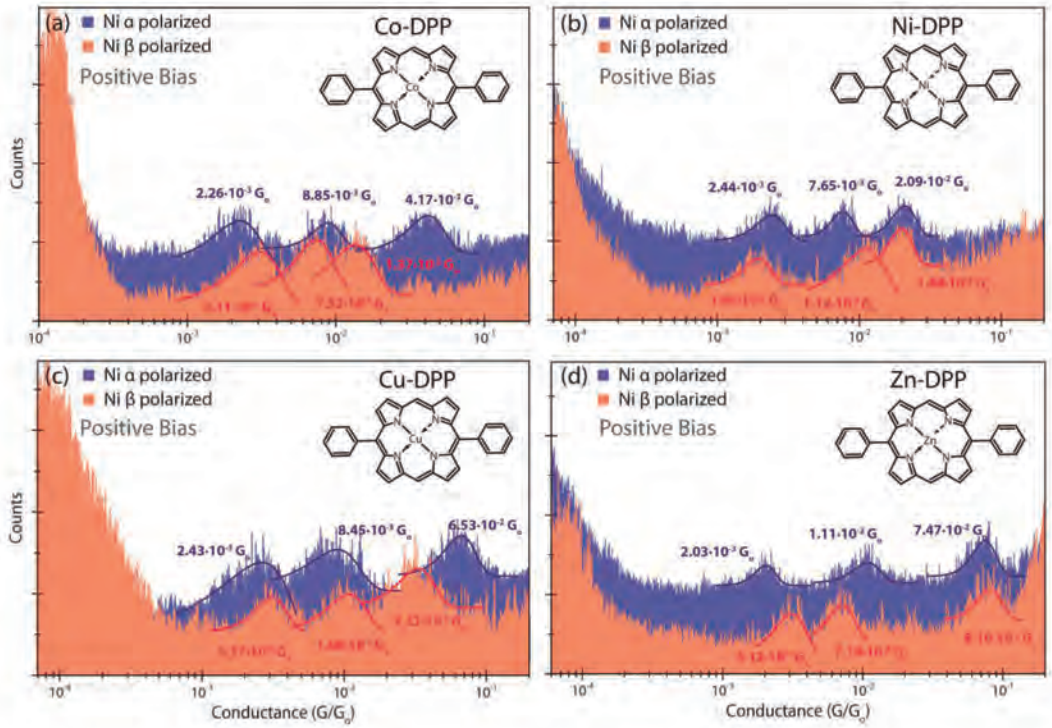

Figure 3 | Single-molecule conductance histograms injecting the electrons from the nickel tip. Schematic single-molecule conductance 1D log-histogram for the metal porphyrins (labelled and represented in the figure) bridging between Au and both α (blue) and β (orange) magnetically polarized Ni tips. Both histograms been vertically offset for clarity. All conductance values have been extracted from Gaussian fits of the peaks. The applied bias was set to +7.5 mV.

The conductance histograms corresponding to the injection of electrons from the nickel tip to the Au substrate (positive bias, see Figure 3) present similar behaviour to the previously obtained in the opposite direction of electron flow (negative bias, Figure 2). Thus, for the Ni-DPP and Zn-DPP without spin-dependent transport are almost identical in the limit of the accuracy of the measurements. However, the two spin-polarized systems (Co-DPP and Cu-DPP) are remarkable because are the first cases reported showing a magnetoresistance effect when the electrons are injected from the magnetic tip. The conductance ratio with the inversion of the magnetization of the nickel tip is approximately 3-fold and 2-fold for Co-DPP and Cu-DPP, respectively. These magnetoresistance values are half of those obtained for the injection from the gold substrate. Figure 4 summarizes the conductance variations of all 4 M-DPP complexes trapped at the tunnelling

junction (Figure 1) for both magnetized (α and β) and non-magnetized Ni STM electrode, and both polarities of the applied voltage bias.

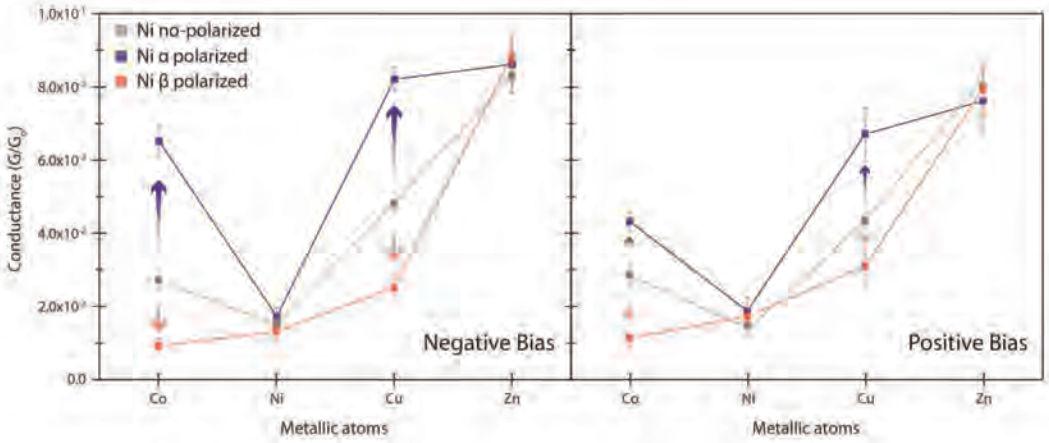

Figure 4 | Yield values (%) of current plateau appearance in single-molecule experiments. Plot of the high conductance (HC) peaks affected by the Ni tip polarization for each M-DPP (indicated in the figure) under non-polarized, α and β polarized Ni tips, represented in grey, blue and orange, respectively. Error bars denote the standard deviation from different experiments

Note that for the single-molecule conductance experiments performed under non-polarized Ni tip electrodes (Figure 4 and Supplementary Information section S1.3), the observed LC, MC and HC values of the non-magnetoresistive molecular junctions (Ni-DPP and Zn-DPP) are invariant in front of the magnetization of the Ni tip electrode. Likewise, [Co-DPP(p4m)$_2$] and [Cu-DPP(p4m)$_2$] presents HC values under non-polarized Ni tip electrodes at intermediate value between the obtained under α and β Ni-tip magnetizations (Figure 4). This "intermediate values "effect can be explained if the injected non-polarized current is understood as an equal injected population of α and β current components with opposite effects over the conductance and a resulting perfect balance between them. (Mmm esto creo k si se puede explicar asi pero habria k ser mas claro, he estado hacienda un sketch k os kiero enseñar a ver si tiene sentido cualitativo)

***Blinking* STM experiments of single-junctions using the [M^{II}(DPP)] complexes (M = Co, Ni, Cu and Zn).** In order to assign the observed magnetoresistance effect in the studied molecular junctions

(Figure 1) as a unique consequence of the Ni-tip polarization, neglecting the effects of the dynamic tapping approach that may lead to stretch-dependent conductance effects, we used a static gap-controlled single-molecule approach based on the spontaneous formation of junctions (*blinking* mode).[16,17] This operation mode records "I vs time" transients at a fixed electrode–electrode separation. When a molecular junction between the functionalized electrodes and the M-DPP molecule is spontaneously formed,[17,19] a current jump or *blink* is observed in the current transient. We refer to this type of experiments to as *blinking experiments*. The blink in this study corresponds to a molecular bridge formation between the pyridine-functionalized STM electrodes and the metalloporphyrin molecule. The blinks typically last for short periods of time (from few hundreds of milliseconds to a second), after which the current suddenly drops due to the stochastic breakdown of the junction.[17,19,28] The formation of mechanically stable molecular junctions during the blinking process was confirmed by an induced molecular breakdown applying a vertical pulling stage over the STM tip.[28] The appearance of plateaus during this pulling sequence ascertains the stretching of the single-molecule bridge because the junction is mechanically forced to break,[29,30] evidencing that the blink was a consequence of the molecular junction formation (Supplementary Information section S2).[9]

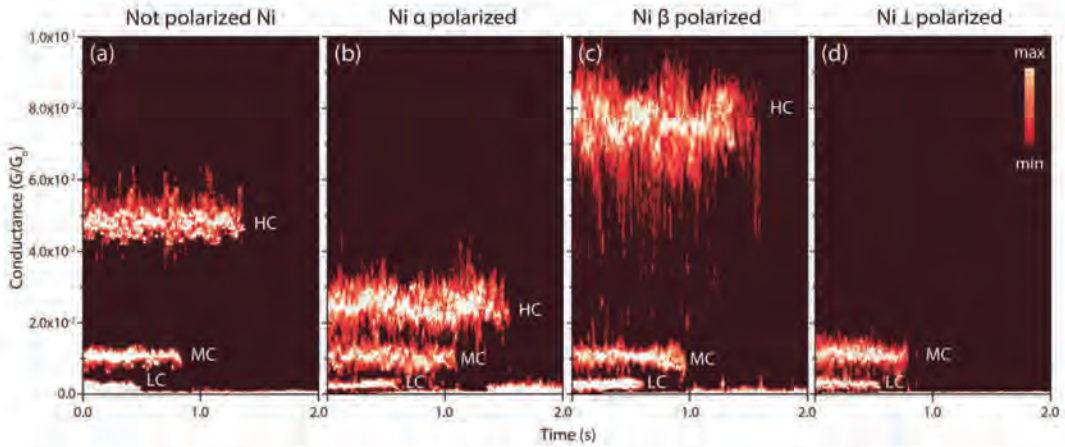

Figure 5 | 2-dimension blinking maps were obtained by accumulating hundreds of blinks at a common time origin of blinking traces Cu-DPP under (a) non-polarized, (b) α-Ni tip, (c) β-Ni-tip and (d) perpendicular polarized electrodes. The 2D-maps were normalized to a color scale versus the total number of counts,

representing 100 counts the maximum and 0 counts the minimum. Applied voltage bias and initial setpoint currents were -7.5 mV and 7 nA, respectively.

We used the low electro-electrode gap separations (ca. 1-1.2 nm) to assure the complexation of the central metal (HC feature appearance) during the single-molecule junction formation.[19,31] For all M-DPP molecules under non-polarized Ni tips, the LC, MC and HC single-molecule conductance values are equivalent to those obtained using the dynamic STM-BJ working mode under the same non-polarized conditions (Figure 2 and Supplementary Information section S2.2). Figure 5 shows 2D maps of hundreds of blinking traces for the Cu-DPP molecule under different Ni magnetization conditions. The observed lifetime of the three conductance ranges for all four molecules are also in accord to the previously reported values (SI 2.2).[19,32] We observe the same behaviour found using the dynamic STM-BJ mode (Figures 2-4): larger HC values under α-Ni tip magnetization (Fig 5b), lower HC values under the β-Ni tip magnetization (Fig 5c) and an intermediate HC value for the non-magnetize Ni tip (Fig. 5a). The above results rule out any stretching effect on the measured single-molecule magnetoresistance effect, which is evident in the HC feature only associated to the conduction thought the metal core.

In order to expand the study of the magnetoresistance effects in the single-molecule junctions, we anted to explore other directions of for the magnetization of the STM Ni electrode. Figure 5D shows a 2D map built out of hundreds of blinking events for the Cu-DPP complex under an applied Ni magnetization along the perpendicular direction to the junction main axis (⊥-Ni).[33] The perpendicular magnetization of the Ni tip acts again over the HC feature only, which is completely washed out from the 2D map under this perpendicular Ni-tip magnetization, meaning that the single-molecule conductance is below the detection limit of our current amplifier ($<10^{-7}$ G_o).[9,10] Based on the Cu-DPP and Co-DPP molecules results, where the LC and MC range present no dependence on the Ni tip polarization unlike the HC range, we can consider a double conductance behaviour of the metalloporphyrins under the effects of the Ni-tip polarization.

Theoretical study of the single-molecule spin-dependent transport. To rationalize the origin of the acute spin-dependent transport observed in the single-molecule contacts with [M^{II}(DPP)] complexes (M = Co, Ni, Cu and Zn) through the metal channel, we performed periodic DFT calculations. The structural models for the calculations consisted in two true semi-infinite Au surface electrodes with the pyridine moieties attached to both Au(111) surface through the thiol S atoms in a three-fold hollow configuration, and the metalloporphyrin block in the conformation selecting the transport metal channel (see Figure 6 inset and more details in the Experimental Methods section). The calculations were carried out using two equivalent gold surfaces to simplify the system and considering that the spin-filter effect arises from the mixing of the gold surface levels with the spin-polarized molecular orbitals. The nickel tip is not included in the calculation since it just controls the final device magnetoresistance because the transport of minority spin carriers is more efficient in the magnetically polarized Ni electrode.

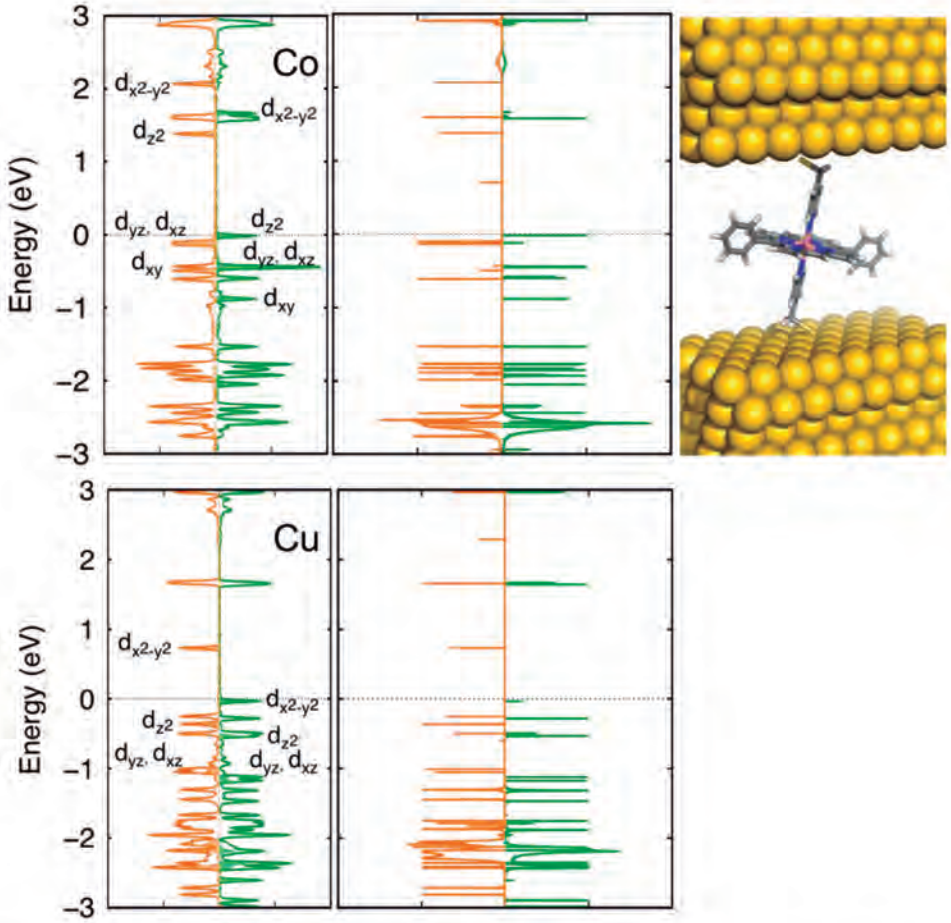

Figure 6 | DFT calculated spin-resolved projected density of states and transmission spectra. (left) DOS of the Co^{II} and Cu^{II} metalloporphyrins (filled curve corresponds to the transition metal levels) and (right) transmission spectra (between 0 and 2 for each spin). Green and orange colors correspond to the alpha and beta spin contributions, respectively.

The calculated density of states (DOS) and transmission curves for the two M-DPP systems showing magnetoresistance (M = Co and Cu) adsorbed between two Au(111) surfaces are plotted in Figure 6. The main observed differences between the two studied cases can be summarized as follow for each metal system:

(i) The Co^{II} system has a low-spin S=1/2 electronic configuration ($d_{xy}^2 d_{xz}^2 d_{yz}^2 d_{z2}^1 d_{x2-y2}^0$), the main contribution to the transport is the highest occupied alpha d_{z2} orbital that appears just below the Fermi level (Figure 6, above) and consequently, the main transport carriers are α holes. Thus, this is in

strike contrast to that found previously in the magnetoresistance effect reported for the $[M(tzpy)_2(NCX)_2]$ complexes (M = Fe and Co, X = S and Se) showing the β empty t_{2g} orbital as main orbital channels. In such cases, the transport carriers are mainly electrons with β spin. This difference is really substantial because the spin of the molecule is aligned with the magnetization of the Ni tip due to the Zeeman effect, and the electron transport in the nickel tip is due to minority carriers. Hence, for instance the $[Fe(tzpy)_2(NCS)_2]$ complex has the spin of the molecule aligned with the tip magnetization, the carriers of the molecule and the tip are the same minority ones (see Figure 7 for a detailed description of the spin involved in the two types of single-molecule junctions). However, for the Co^{II} metalloporphyrins with majoritary carriers, the magnetoresistance effects are lower than in $[Fe(tzpy)_2(NCS)_2]$ complexes because the carriers of the two subsystem (tip and molecule) are always different. From the experimental point of view, such differences are reflected in the direction of the magnetization of the Ni tip showing the maximum conductance value, down for all $[M(tzpy)_2(NCX)_2]$ complexes and up for the $[CoDPP(p4m)_2]$ system (see Figure 2).

(ii) The Cu^{II} case has a low-spin S=1/2 electronic configuration ($d_{xy}^2 d_{xz}^2 d_{yz}^2 d_{z^2}^2 d_{x^2-y^2}^1$) with a singly occupied alpha $d_{x^2-y^2}$ orbital as the major contributor to the transport channel. The situation is analogous to that found in the case of the Co^{II} single-molecule junction. The transport is again due to the majority carriers, α holes if the molecular spin is up. Experimentally, the behaviour is identical to that of the Co-DPP case (see Figure 2) showing also the maximum of conductance with the magnetization down for the Ni tip.

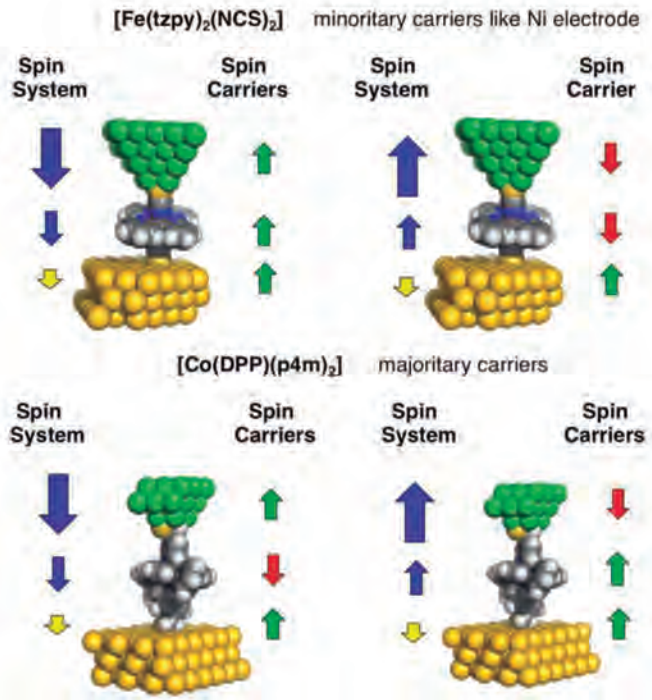

Figure 7 | Spin of the electrodes and molecule in the two-types of single-molecule junctions. In the $[Fe(tzpy)_2(NCS)_2]$ system the molecule has minority carriers, as the nickel tip. Thus, if we assume a fixed spin orientation for the gold substrate when the molecule and tip electrodes are down, the spin of the carriers is the same in the three subsystems leading to a high magnetoresistance effect. However, such situation cannot be reach in the $[CoDPP(p4m)_2]$ metalloporphyrin because always the spins of carriers in the tip and molecule are the opposite, leading to intermediate magnetoresistance effects.

Figure 8 shows the comparison of the experimental and theoretical conductance values. It is well know the drawback of DFT methods to reproduce quantitatively the experimental data, thus, our results considering the model with metal coordination 6 (two axial ligands) for the Co-DPP, Ni-DPP and Cu-DPP systems and 5 (only one axial ligand) for Zn-DPP give a similar qualitative description of the variation of the conductance found experimentally. One of the most important problems in such calculations is the lack of an accurate structure of the tip-molecule-substrate system in the exact moment that the measure is performed. DFT results properly reproduce the trend of the increasing conductance for the series of Ni-DPP, Cu-DPP and Zn-DPP systems (see Supplementary Information section S5 for transmission curves for the diamagnetic systems). However, the value obtained for

Co-DPP the conductance value is too high. In this case, it is the unique system where the main channel for the electron transport is that related with the d_{z^2} orbital (as discussed above, see Figure 6). Hence, a small change in the M-N distance from the equilibrium in the interaction with the STM tip could cause significant changes in the calculated values. Thus, such value is very sensitive to small changes in the model employed in the calculations.

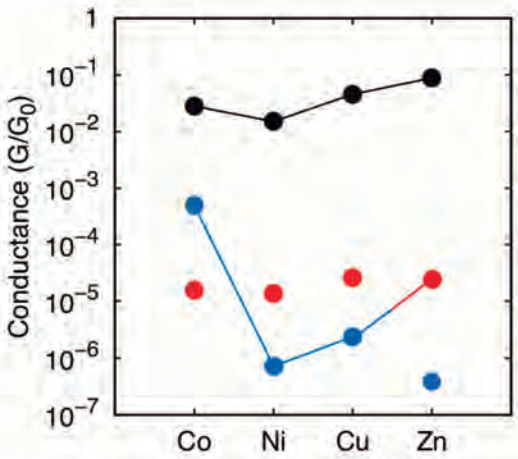

Figure 8 | Experimental and DFT calculated conductance values for the single-molecule junctions. The experimental values are indicated in black, the calculated values using a PBE+U functional with a hexaccordinates model (two axial p4m ligands) in blue while the results with only one axial ligand are indicated in red color.

CONCLUSIONS

Here, we present an example of magnetoresistance in a single-molecule device at room temperature using metalloporphyrin complexes showing the largest conductance measured in comparison with the previous reported systems. The electronic structure of the metal centres has a crucial role. Only the paramagnetic systems Co-DPP and Cu-DPP complexes present magnetoresistance effect. For these two systems, the main transport channel is due to the alpha singly-occupied d_{z^2} and $d_{x^2-y^2}$ orbitals, respectively. The electron transport is due to majority alpha holes systems while for the

previously reported systems, the carriers were minority beta electrons. Such difference has a strong impact, (i) the magnetoresistance effect appears for any bias sign, either injecting the electrons from the gold substrate or the nickel tip and (ii) the maximum of conductance in the magnetoresistance devices is reached with an alpha polarization of the magnetic tip while for previously reported cases the magnetoresistance effect always was found by injecting from the gold substrate and using beta magnetization of the magnetic tip. Furthermore, the magnetoresistance is strongly dependent on the direction of the tip magnetic polarization. Also, we present in this work the first experiments applying a perpendicular field to the transport pathways. Such tip magnetization completely blocks the transport through the metal channels with large orbital participation of the paramagnetic centres Consequently, large anisotropy with the direction of the magnetization of the nickel tip is found. These experiments demonstrate the crucial role of the electronic structure of the magnetic molecule and its interactions with the electrodes, the Spinterface. The use of transition metal complexes opens a large variety of options concerning the carriers-type (their spin, energy and electron/hole nature) to tune the transport properties on future magnetoresistance spintronic single-molecule devices.

EXPERIMENTAL METHODS

Sample preparation. Pyridin-4-yl-methanethiol was synthesized as described previously by Puigmarti-Luis et. al. Co-DPP and Zn-DPP molecules were synthesized according to the procedure described by Song et al. Based on this procedure, changing the solvent and reaction times, Cu-DPP and Ni-DPP molecules were synthetized, for more details see synthesis section.

All glassware and PFTE STM cells were cleaned with piranha solution (3:1 H_2SO_4/H_2O_2 by volume) before usage followed by rinsing with 18 MΩ cm^{-1} Milli-Q water (Millipore). An Au (111) single crystal substrate (10 mm x1 mm) of 99.9999% purity and orientation accuracy < 0.1 degrees was purchased from MaTeck (Germany). Before each experiment, the single crystal Au (111) substrate was electropolished to eliminate possible residual contamination and then annealed with a H_2 flame. The surfaces were then washed with argon-purged ethanol and dried under a stream of argon after

which they were placed in 0.8-1 mM ethanol solution of pyridin-4-yl-methanethiol for 24 h. Ni tips were mechanically cut, coated with Au, immersed in 0.8-1 mM ethanol solution of pyridin-4-yl-methanethiol for 24 h, washed thoroughly with ethanol and dried under a stream of argon and then magnetized for 2h (see section). The Au (111) surface, after the functionalization step, was also washed thoroughly with ethanol and dried under a stream of argon. The Au (111) surface was then assembled in the STM cell and the surface electrode filled with a 80 μL of pure mesitylene, where STM junction control experiments were firstly run. Next, few drops of a 8-12 nM mesitylene solution of the M-DPP was added to build the porphyrin mediated molecular wires.

Conductance measurements. An STM-BJ method was employed to build and characterize charge transport through single-molecule wires built with the different metal complexes studied in this work. The two biased electrodes of the molecular junction, a Au(111) single crystal (99.9999% Mateck, Germany) and a mechanically cut polycrystalline Ni wire (99.99%, Goodfellow, UK) were used as the support and the STM top electrodes, respectively. In a regular STM-BJ experiment (see manuscript), the Ni tip was repeatedly driven onto the Au surface while simultaneously monitoring the current flowing between them. Several thousands (~5000) retraction curves were then stored and used to build the conductance histogram of the single-molecule device. Because not every curve displayed plateau features corresponding to the molecular quantum conductance of the single-molecule bridge, we designed an automatic algorithm that identify and select curves containing such single-molecule features. The exact same selection criteria were applied throughout all measured series. To avoid the Ni wire oxidation under ambient conditions, the prepared Ni electrode was magnetically polarized and stored under in anaerobic conditions before use, as we report in previous works.[21] All experiments were conducted in an organic solvent (mesitylene) with very low oxygen and water solubility.

Technical details of the dynamic Break-Junction experiments. Details about the STM-break junction technique are published elsewhere.[30] All experiments were carried out with a homemade PTFE-STM cell and a PicoSPM II microscope head controlled using a PicoScan 2500 electronics,

all from Agilent (USA). The STM head was mechanically and electronically isolated. Data was acquired using a NI-DAQmx/BNC-2110 National Instruments (LabVIEW data acquisition System, USA) and analyzed with our own LabVIEW code. In a typical break-junction experiment, the STM tip is first brought to a tunneling distance over a flat clean metallic surface area. The STM feedback is then turned off and the tip is driven in and out of contact with the substrate at a speed of 1-2 V/s. This 2-points feedback loop is used to collect thousands of current decays (5000-6000) during the tip pulling cycles. In order to minimize possible mechanical disruption of the tip and sample surfaces, the reached maximum current in the 2-points feedback loop was set to a low value well below saturation, which prevented the STM tip crashing against the substrate electrode. 10-15% of the collected current decays display steps or *plateaus*, and are used to determine the single molecule conductance using the expression $G=I_{step}/U_{bias}$ where G is the conductance, I the current and U is the potential difference between the tip and substrate electrodes. The current decays are accumulated to form linear conductance histograms. The observed peaks in the conductance histograms correspond to the observed plateaus in the current decays and provide averaged single-molecule conductance values. An automated selection process designed by own LabVIEW code was used to select the decays that showed plateaus from the ones that did not. The user defines the initial selection criteria that are fixed throughout all the experimental series.

Technical details of the static *blinking* experiments. The *blinking* captures (tens of curves) were accumulated into 2D maps during a total time of 6h for each experiment.[34,48] No selection procedures were applied at this time and so all *blinking* events are used to build the 2D histograms. In order to compare the lifetimes of the blinks in the 2D maps, all the samples were set into a common time origin and baseline. The final STM tip pulling after the *blinking* was performed by externally controlling the piezo Z-position (see Supplementary Information section 5).

Computational details. Electron transport calculations were carried out with the molecule sandwiched between five gold layers with a 5 x 4 surface unit cell using the Siesta[34] and Gollum[35] codes with the PBE[36]+U functional (U = 4.0 eV), a $1e^-$ pseudopotential for the gold[37] atom while

double-ζ basis set with polarization for the other elements. For the transition metals, a small core pseudopotential was used, thus, the orbitals 3s and 3p were considered within the basis sets. The structures of the M-DPP metalloporphyrins interacting with the pyridin-4-yl-methanethiol axial ligands that are necessary for the transport calculations were obtained from DFT calculations B3LYP[38] functional with a TZVP basis for H, C, N and S and QZVP basis set for metal atoms by means of the Gaussian09 package.[39] The key structural parameter is M-N distance with the pyridine ligand, d(Co-N) = 2.432 Å, d(Ni-N) = 2.306 Å, d(Cu-N) = 2.728 Å, d(Zn-N) = 2.494 Å (see Supplementary Information for a detailed list of cartesian coordinates). In the case of the Ni-DPP system coordinated to the two axial pyridin-4-yl-methanethiol ligands, also the TPSSh[40] functional was employed because it provides better estimation of the state energies than the B3LYP one. Model systems were constructed from previously optimized molecules, attaching 3 gold atoms to each S thiol end with a S-Au distance of 2.2 Å (hollow position). The calculations were performed assuming an homolytic breaking of thiol S-H bond. A triplet state was considered for the remaining S· radical groups.[41] The distance of 4.0 Å between the Zn-DPP molecule plane to the gold surface (on top position) for the pentacordinated system was previously reported.[42–44]

References

1. Urdampilleta, M. *et al.* Molecular Quantum Spintronics: Supramolecular Spin Valves Based on Single-Molecule Magnets and Carbon Nanotubes. *Int. J. Mol. Sci.* **12,** 6656–6667 (2011).
2. Iancu, V., Deshpande, A. & Hla, S.-W. Manipulating Kondo Temperature via Single Molecule Switching. *Nano Lett.* **6,** 820–823 (2006).
3. Accorsi, S. *et al.* Tuning Anisotropy Barriers in a Family of Tetrairon(III) Single-Molecule Magnets with an S = 5 Ground State. *J. Am. Chem. Soc.* **128,** 4742–4755 (2006).
4. Ray, S. G., Daube, S. S., Leitus, G., Vager, Z. & Naaman, R. Chirality-induced spin-selective properties of self-assembled monolayers of DNA on gold. *Phys. Rev. Lett.* **96,** 36101 (2006).
5. Vager, Z. & Naaman, R. Surprising electronic-magnetic properties of close-packed organized organic layers. *Chem. Phys.* **281,** 305–309 (2002).
6. Naaman, R. & Waldeck, D. H. Chiral-Induced Spin Selectivity Effect. *J. Phys. Chem. Lett.* **3,** 2178–2187 (2012).

7. Vager, Z. & Naaman, R. Surprising electronic–magnetic properties of close-packed organized organic layers. *Chem. Phys.* **281,** 305–309 (2002).
8. Aragonès, A. C. *et al.* Measuring the Spin-Polarization Power of a Single Chiral Molecule. *Small* **13,** 1602519 (2017).
9. Aragonès, A. C. *et al.* Large Conductance Switching in a Single-Molecule Device through Room Temperature Spin-Dependent Transport. *Nano Lett.* **16,** 218–226 (2016).
10. Aragonès, A. C. *et al.* Metal-Controlled Magnetoresistance at Room Temperature in Single-Molecule Devices. *J. Am. Chem. Soc.* jacs.6b11166 (2017). doi:10.1021/jacs.6b11166
11. Mannini, M. *et al.* Magnetic memory of a single-molecule quantum magnet wired to a gold surface. *Nat. Mater.* **8,** 194–197 (2009).
12. Sinova, J., Valenzuela, S. O., Wunderlich, J., Back, C. H. & Jungwirth, T. Spin Hall effects. *Rev. Mod. Phys.* **87,** 1213–1260 (2015).
13. Xu, B. & Tao, N. J. Measurement of single-molecule resistance by repeated formation of molecular junctions. *Science* **301,** 1221–3 (2003).
14. Tao, N. J. Electron transport in molecular junctions. *Nat. Nanotechnol.* **1,** 173–181 (2006).
15. Chen, F., Hihath, J., Huang, Z., Li, X. & Tao, N. J. Measurement of Single-Molecule Conductance. *Annu. Rev. Phys. Chem.* **58,** 535–564 (2007).
16. Nichols, R. J. *et al.* The experimental determination of the conductance of single molecules. *Phys. Chem. Chem. Phys.* **12,** 2801–15 (2010).
17. Aragonès, A. C. *et al.* Electrostatic catalysis of a Diels–Alder reaction. *Nature* **531,** 88–91 (2016).
18. Amdursky, N., Pecht, I., Sheves, M. & Cahen, D. Electron Transport via Cytochrome C on Si–H Surfaces: Roles of Fe and Heme. *J. Am. Chem. Soc.* **135,** 6300–6306 (2013).
19. Aragonès, A. C. *et al.* Highly conductive single-molecule wires with controlled orientation by coordination of metalloporphyrins. *Nano Lett.* **14,** 4751–6 (2014).
20. Inkpen, M. S. *et al.* New Insights into Single-Molecule Junctions Using a Robust, Unsupervised Approach to Data Collection and Analysis. *J. Am. Chem. Soc.* **137,** 9971–9981 (2015).
21. Li *et al.* Thermally Activated Electron Transport in Single Redox Molecules. *J. Am. Chem. Soc.* **129,** 11535–11542 (2007).
22. Hines, T. *et al.* Controlling formation of single-molecule junctions by electrochemical reduction of diazonium terminal groups. *J. Am. Chem. Soc.* **135,** 3319–22 (2013).
23. Chen, F. & Tao, N. J. Electron transport in single molecules: from benzene to graphene. *Acc. Chem. Res.* **42,** 429–38 (2009).
24. *Ionic Interactions in Natural and Synthetic Macromolecules*. *Ionic Interactions in Natural and Synthetic Macromolecules* (John Wiley & Sons, Inc., 2012). doi:10.1002/9781118165850
25. Corden, B. B., Drago, R. S. & Perito, R. P. Steric and electronic effects of ligand variation on cobalt dioxygen catalysts. *J. Am. Chem. Soc.* **107,** 2903–2907 (1985).
26. Arnold, L., Norouzi-Arasi, H., Wagner, M., Enkelmann, V. & Müllen, K. A porphyrin-related macrocycle from carbazole and pyridine building blocks: synthesis and metal coordination. *Chem. Commun. (Camb).* **47,** 970–2 (2011).
27. Wong, W.-Y. Metallated molecular materials of fluorene derivatives and their analogues. *Coord. Chem. Rev.* **249,** 971–997 (2005).
28. Aragonès, A. *et al.* Detection of Single-Molecule Reaction Using STM Approach. *Protoc. Exch.* (2016). doi:10.1038/protex.2016.013
29. Haiss, W. *et al.* Measurement of single molecule conductivity using the spontaneous formation of molecular wires. *Phys. Chem. Chem. Phys.* **6,** 4330–4337 (2004).
30. Díez-Pérez, I. *et al.* Rectification and stability of a single molecular diode with controlled orientation. *Nat. Chem.* **1,** 635–641 (2009).
31. Ponce, I. *et al.* Building Nanoscale Molecular Wires Exploiting Electrocatalytic Interactions.

Electrochim. Acta **179,** 611–617 (2015).
32. Noori, M. *et al.* Tuning the electrical conductance of metalloporphyrin supramolecular wires. *Sci. Rep.* **6,** 37352 (2016).
33. Li, J.-J. *et al.* Giant Single-Molecule Anisotropic Magnetoresistance at Room Temperature. *J. Am. Chem. Soc.* **137,** 5923–5929 (2015).
34. Soler, J. M. *et al.* The SIESTA method for *ab initio* order- *N* materials simulation. *J. Phys. Condens. Matter* **14,** 2745–2779 (2002).
35. Ferrer, J. *et al.* GOLLUM: a next-generation simulation tool for electron, thermal and spin transport. *New J. Phys.* **16,** 93029 (2014).
36. Perdew, J. P., Burke, K. & Ernzerhof, M. Generalized Gradient Approximation Made Simple. *Phys. Rev. Lett.* **77,** 3865–3868 (1996).
37. Toher, C. & Sanvito, S. Effects of self-interaction corrections on the transport properties of phenyl-based molecular junctions. *Phys. Rev. B* **77,** 155402 (2008).
38. Becke, A. D. Density-functional thermochemistry. III. The role of exact exchange. *J. Chem. Phys.* **98,** 5648–5652 (1993).
39. Frisch, M. J. *et al.* Gaussian 09, Revision D.01. *Gaussian Inc.* Wallingford CT (2009). doi:10.1159/000348293
40. Tao, J., Perdew, J. P., Staroverov, V. N. & Scuseria, G. E. Climbing the Density Functional Ladder: Nonempirical Meta–Generalized Gradient Approximation Designed for Molecules and Solids. *Phys. Rev. Lett.* **91,** 146401 (2003).
41. Bencini, A., Rajaraman, G., Totti, F. & Tusa, M. Modeling thiols on Au(111): Structural, thermodynamic and magnetic properties of simple thiols and thiol-radicals. *Superlattices Microstruct.* **46,** 4–9 (2009).
42. Mielke, J. *et al.* Adatoms underneath Single Porphyrin Molecules on Au(111). *J. Am. Chem. Soc.* **137,** 1844–1849 (2015).
43. Kim, H. *et al.* Mapping the electronic structures of a metalloporphyrin molecule on Au(111) by scanning tunneling microscopy and spectroscopy. *Phys. Rev. B* **80,** 245402 (2009).
44. Yokoyama, T., Yokoyama, S., Kamikado, T. & Mashiko, S. Nonplanar adsorption and orientational ordering of porphyrin molecules on Au(111). *J. Chem. Phys.* **115,** 3814–3818 (2001).

Acknowledgements

The research reported here was supported by the Spanish *Ministerio de Economía y Competitividad* (MINECO) (grants CTQ2015-64579-C3-1-P, CTQ2015-64579-C3-3-P, CTQ2015-71406-ERC). E.R. thanks Generalitat de Catalunya for an ICREA Academia award. I. D.-P. thanks the Ramon y Cajal program (MINECO) for financial support. D.A. thanks CONICYT + PAI "Concurso nacional de apoyo al retorno de investigadores/as desde el extranjero, convocatoria 2014 82140014" for financial support. D.A. thanks Centers of Excellence with Basal/CONICYT financing, grant FB0807, CEDENNA. Powered@NLHPC: This research was partially supported by the supercomputing infrastructure of the NLHPC (ECM-02). The authors acknowledge the general

facilities of the University of Barcelona (CCiT-UB) and the computer resources, technical expertise and assistance provided by the Barcelona Supercomputing Centre.

Author contributions

A. C. A., F. S. and I. D.-P. performed the single-molecule transport measurements. A. G. C. and N. A. A. synthesized the metalloporphyrin complexes and characterized them. A. M. R., D. A. and E.R. performed the theoretical calculations. E. R. and I. D.-P. conceived the idea, supervised the project and wrote the paper.

Additional information

Supplementary Information, chemical compound information and sample preparation information are available in the online version of the paper. Reprints and permissions information is available online at www.nature.com/reprints. Correspondence and requests for materials should be addressed to I.D.-P. and E.R.

Competing financial interests

The authors declare no competing financial interest.

Supporting information (SI)

Identifying spin-dependent electron pathways in supramolecular metalloporphyrin wires

Albert C. Aragonès, Alejandro Martín-Rodríguez, Arantzazu Gonzalez Campos, Núria Aliaga-Alcalde, Daniel Aravena, Fausto Sanz, Eliseo Ruiz, Ismael Díez-Pérez

Table of contents

1. Break-junction single-molecule transport measurements

1.1. Representative pulling curves

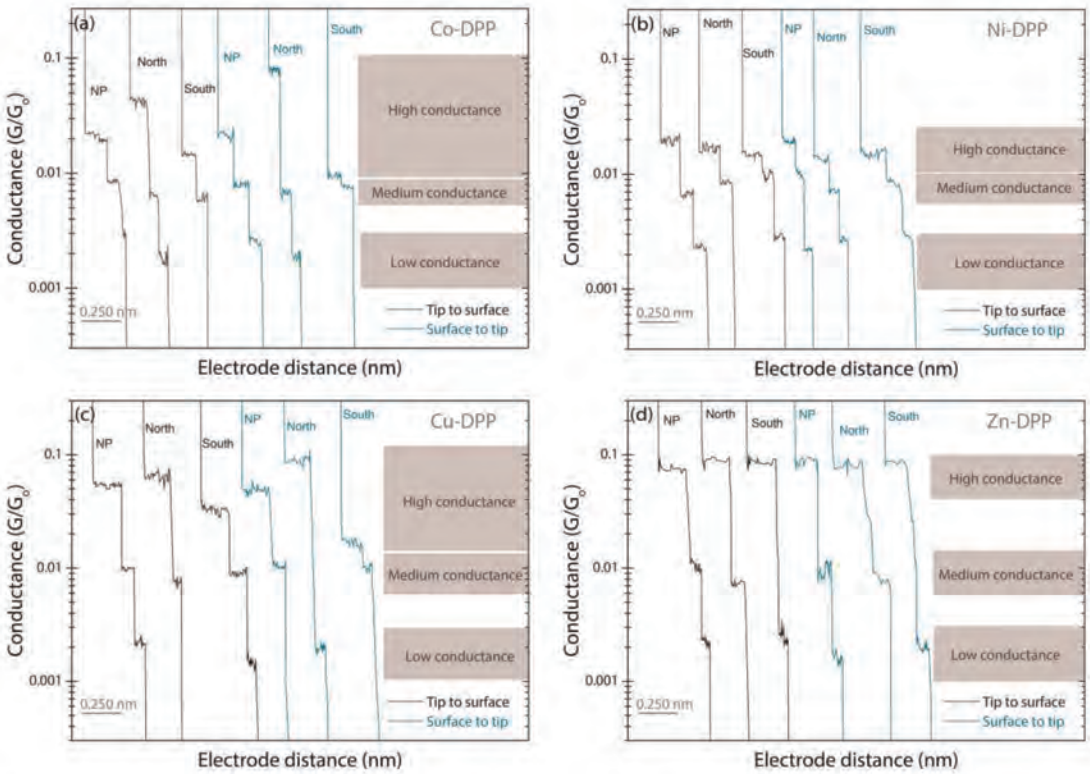

Fig. S1.1 Representative BJSTM single current decay curves in semi-log scale captured during the retraction stage and used to build the 1D semi-log conductance histograms. The applied bias was set to −7.5 mV or +7.5mV depending the applied current sense direction.

1.2. 1D histograms of non-polarized measurements: injecting from the Au

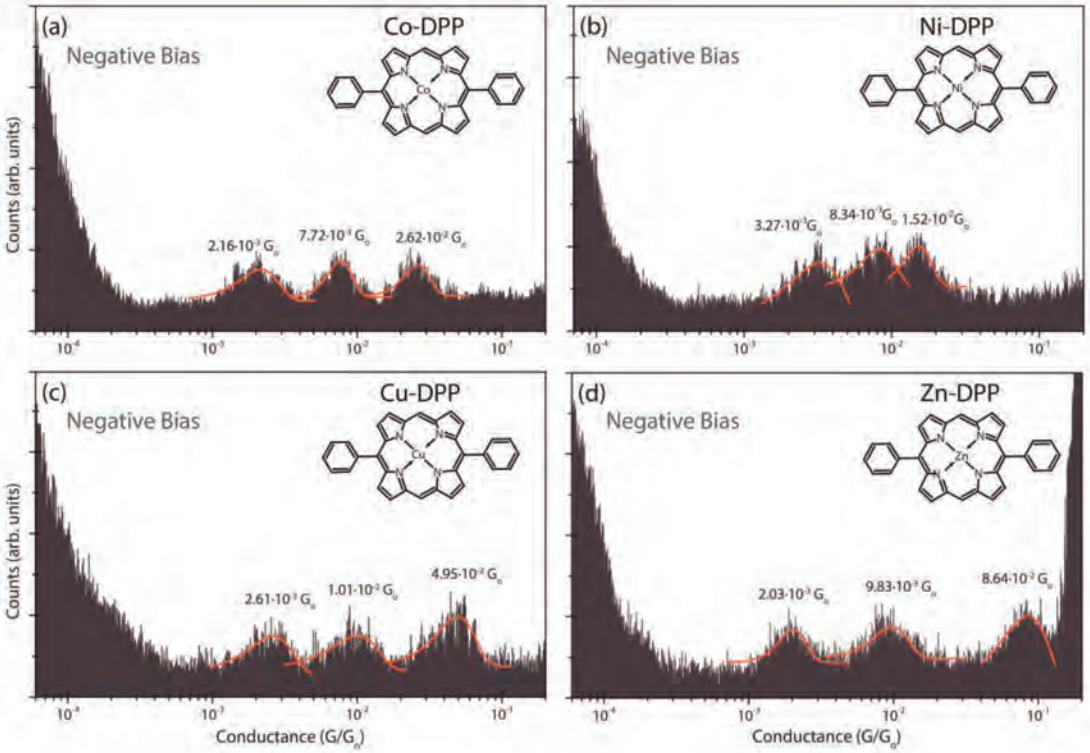

Fig. S1.2 Schematic single-molecule conductance 1D log-histogram for the metal porphyrins (labeled and represented in the figure) bridging between Au and non-polarized Ni tips. All conductance values have been extracted from Gaussian fits of the peaks. The applied bias was set to −7.5 mV.

1.3. 1D histograms of non-polarized measurements: injecting from the Ni

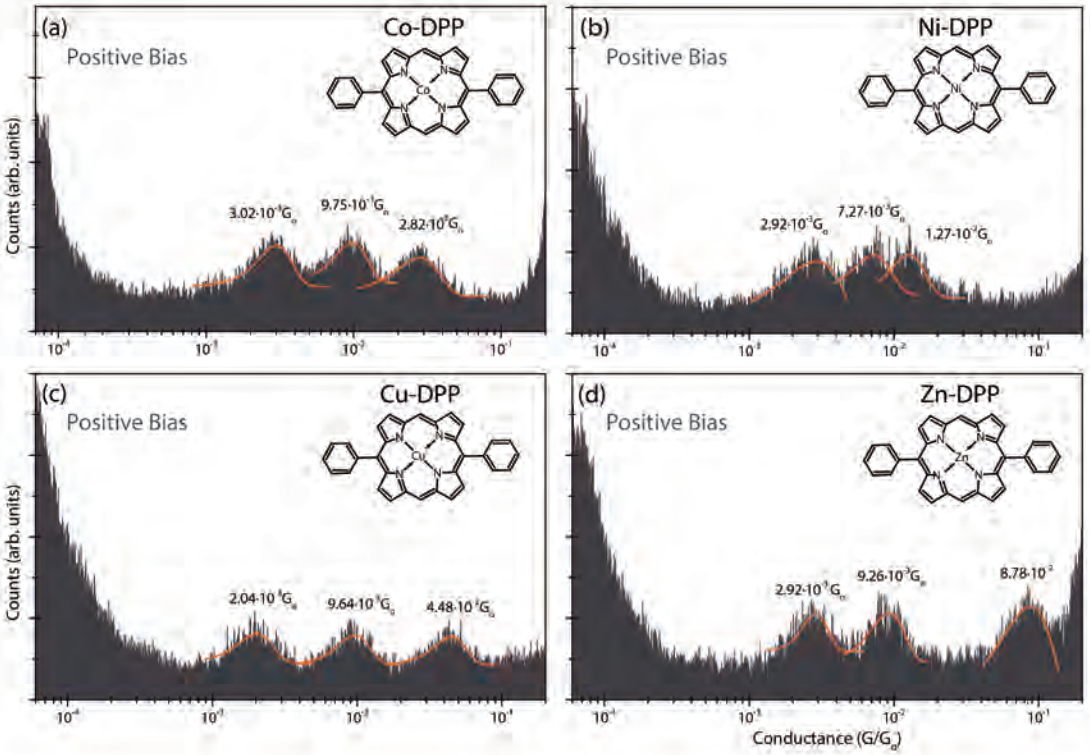

Fig. S1.3 Schematic single-molecule conductance 1D log-histogram for the metal porphyrins (labeled and represented in the figure) bridging between Au and non-polarized Ni tips. All conductance values have been extracted from Gaussian fits of the peaks. The applied bias was set to +7.5 mV.

1.4. 1D histograms of polarized measurements for the modified porphyrins

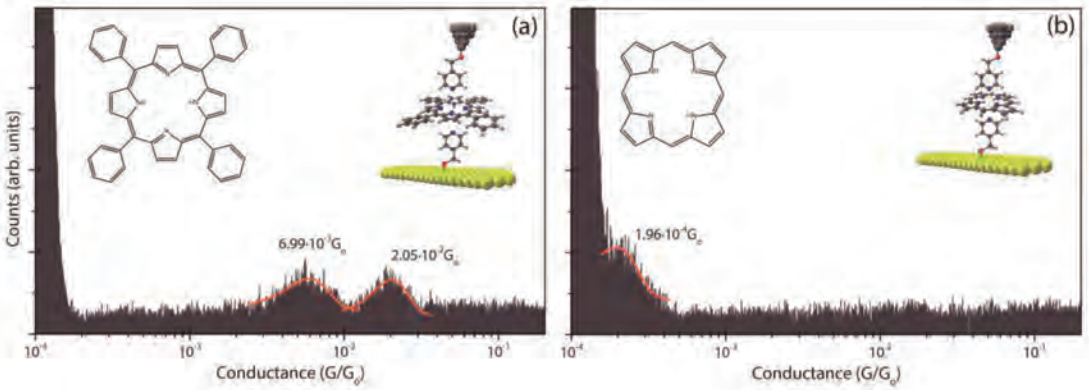

Fig. S1.5 Schematic single-molecule conductance 1D log-histogram for the l porphyrins (labeled and represented in the figure) bridging between functionalized Au substrate and nonpolarized Ni tips. All conductance values have been extracted from Gaussian fits of the peaks. The applied bias was set to −7.5 mV.

1.5. 1D histograms of polarized measurements with non-functionalized tip electrodes

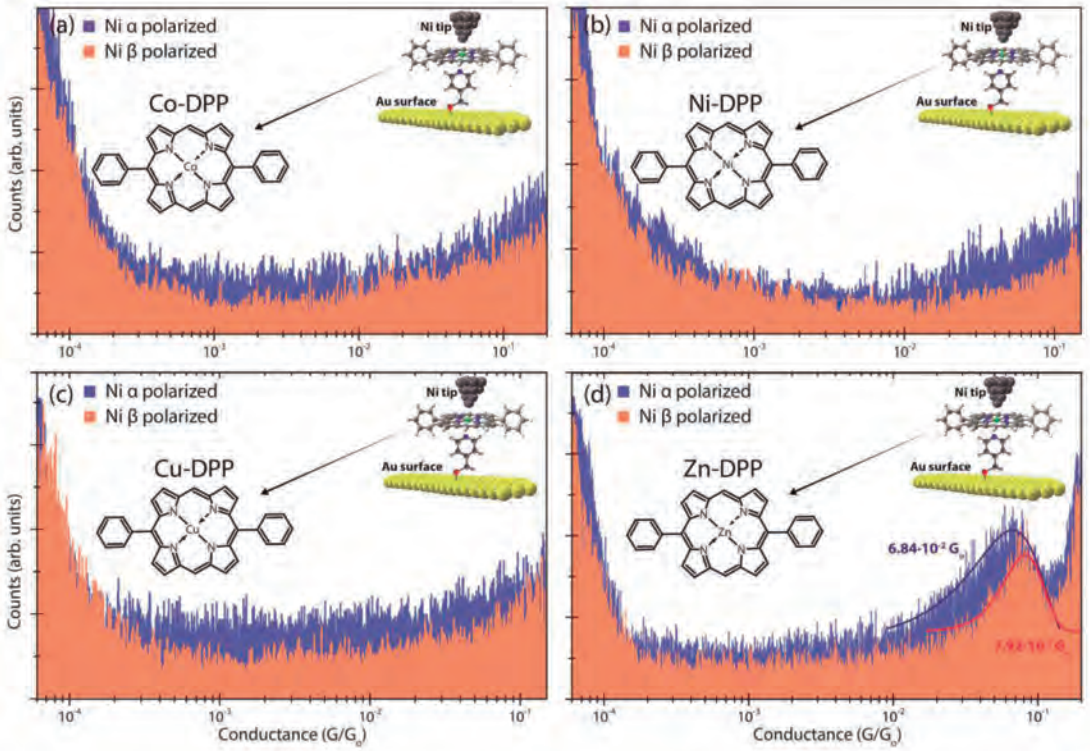

Fig. S1.5 Schematic single-molecule conductance 1D log-histogram for the metal porphyrins (labeled and represented in the figure) bridging between functionalized Au substrate and both α (blue) and β (orange) magnetically polarized Ni tips in the absence of the pyridinyl units. Both histograms been vertically offset for clarity. All conductance values have been extracted from Gaussian fits of the peaks. The applied bias was set to −7.5 mV.

1.6. 1D histograms of control tapping experiments

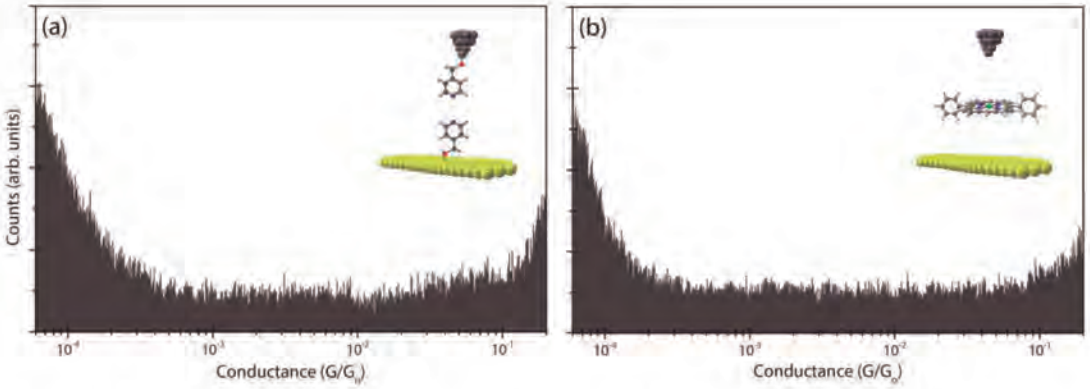

Fig. S1.6 Schematic single-molecule conductance 1D log-histogram for the experiments in the absence of molecule with both tip and surface functionalized with pyridinyl groups (a) and in the absence of the pyridinyl units at the tip and substrate electrodes surfaces when Cu-DPP is present in solution (b).

2. Blinking single-molecule transport measurements

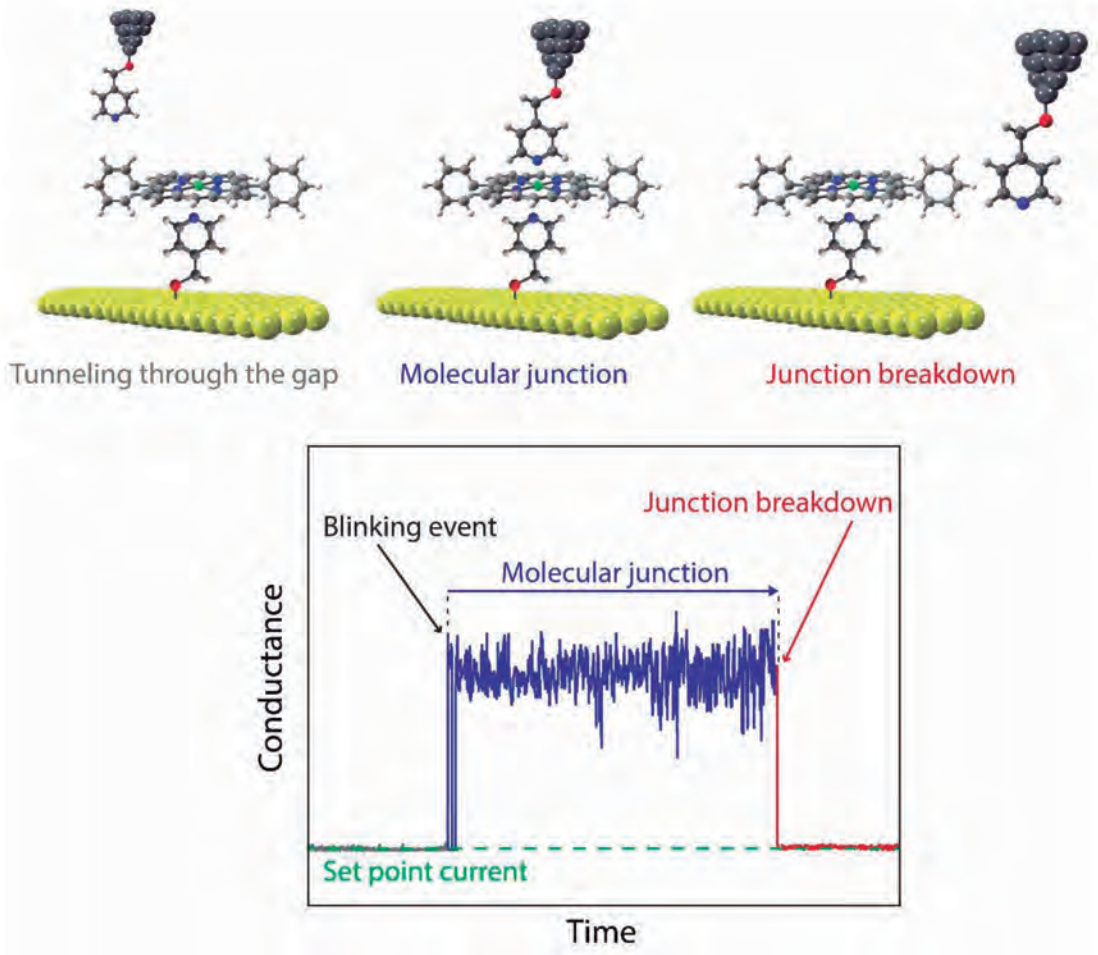

Fig. S2 Schematic of the STM junction experiment describing the formation and breakdown of a metalloporphyrin junction.

2.1. Blinking events samples

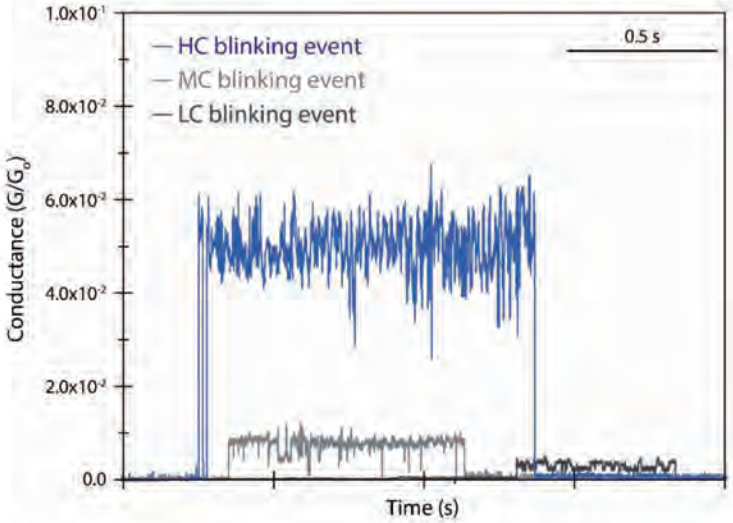

Fig. S2.1 Representative individual "blinks" corresponding to the formation of molecular junctions with the Cu-DPP molecule showing the 3 conductance ranges labelled on the figure.

2.2. 2D maps of non-polarized measurements: injecting from the Au

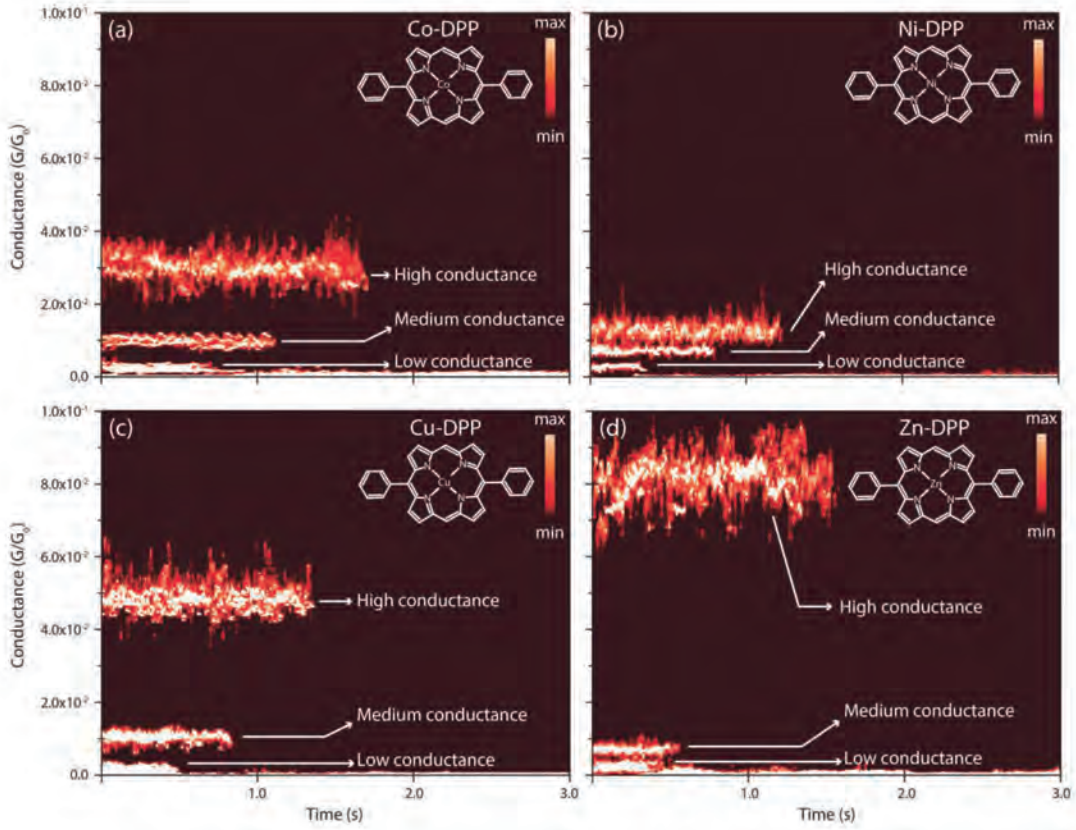

Fig. S2.2 2D blinking maps of the metal porphyrins (labeled and represented in the figure) bridging between Au and non-polarized Ni tips, obtained by accumulating hundreds of blinks at a common time origin of blinking traces. The 2D-maps were normalized to a color scale versus the total number of counts, representing 100 counts the maximum and 0 counts the minimum. Applied voltage bias and initial setpoint currents were -7.5 mV and 7 nA, respectively.

2.3. Control blinking experiments

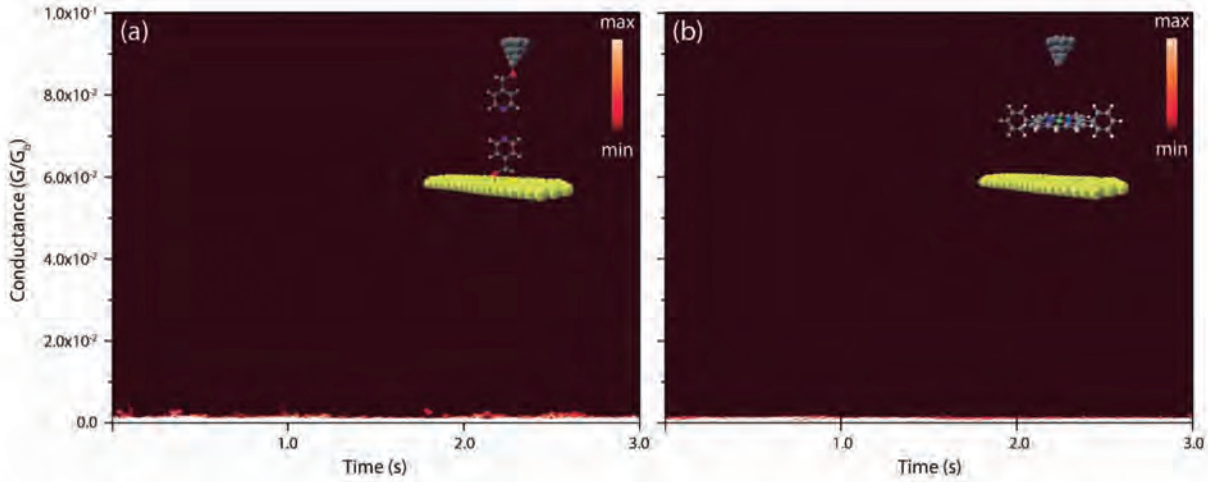

Fig. S2.3 Schematic single-molecule conductance 1D log-histogram for the experiments in the absence of molecule with both tip and surface functionalized with pyridinyl groups (a) and in the absence of the pyridinyl units at the tip and substrate electrodes surfaces when Cu-DPP is present in solution (b).

2.4. Pulling curves

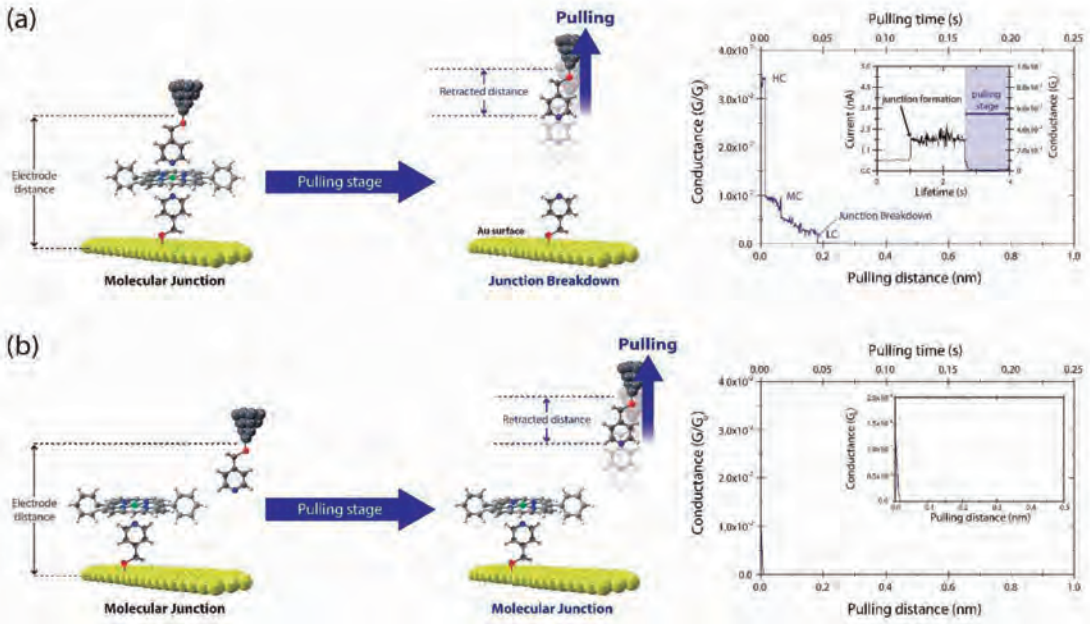

Fig. S2.4 (a) Pulling exerted after the spontaneous junction breakdown showing immediate exponential decay without mechanical resistance suggesting the absence of a molecular junction at this stage. (b) Pulling exerted when the current is showing only the tunneling current background without a metalloporphyrin molecule bridged connected between the electrodes which results immediately in an exponential decay in the current without any mechanical resistance.

3. Characterization of the Ni tip magnetization

The magnitude of the magnetic polarization of the Ni tip was characterized before and after the STM experiment using SQUID magnetometry to assure that the Ni magnetization persisted over the entire timeframe of the experiments (Fig. S4). The direction of the polarized Ni tips was also characterized following the procedure used in previous works.[1] To avoid the Ni wire oxidation during the polarization procedure and transport measurements under ambient conditions, the prepared Ni electrode was magnetically polarized and stored in strict anaerobic conditions before use. The Ni tip oxidation has been monitored during use by ex situ SEM-EDS electric microscopy.[1] Before the tip functionalization it is transferred to the STM cell, and driven several times towards the Au surface to get a light Au coating that protects the tip apex surface against further oxidation throughout the timeframe of all the single-molecule transport experiments and enhance the pyridin-4-yl-methanethiol functionalization

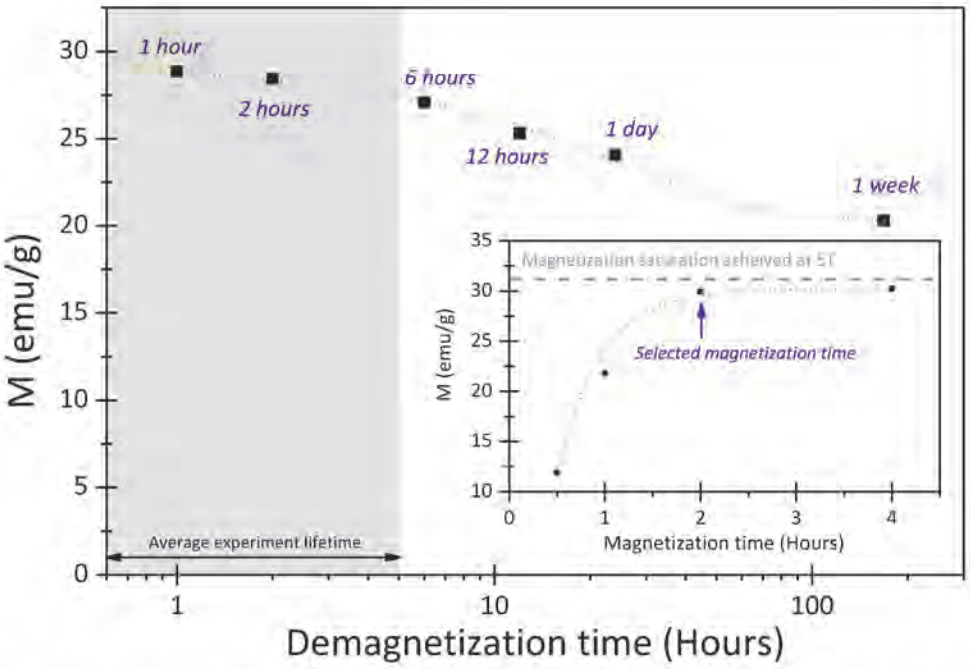

Fig. S4 SQUID measurements of different demagnetization times of Ni tips. Inset shows different magnetization times for Ni tips using the setup described in the manuscript and compared to the magnetization value achieved by the SQUID.

4. Additional technical details of the single-molecule transport measurements

Details about the STM-break junction technique (BJSTM) are published elsewhere. [2,3] All experiments were carried out with a homemade PFTE-STM cell and a PicoSPM II microscope head controlled using a Picoscan 2500 electronics, all from Agilent (USA). The STM head was mechanically and electronically isolated. Data was acquired using a NI-DAQmx/BNC-2110 National Instruments (LabVIEW data acquisition System, USA) and analyzed with LabVIEW code. In a typical BJSTM, the STM tip is first brought to tunneling distance over a flat clean Au (111) surface area. The STM feedback is then turned off and the tip is driven into and out of contact with the substrate at 1 V/s. These 2-points feedback loop is used to collect thousands of current decays (4000-5000) during the tip pulling cycles.[4] In order to minimize disruption of the tip and sample surface functionalization, the attained maximum current in the 2-points feedback loop was set to a low value well below saturation, which prevented the STM tip crashing against the substrate electrode. 15-20% of the collected current decays display steps (plateaus),[1,3,5–7] and are used to determine the single molecule conductance using the expression $G=I_{step}/U_{bias}$ where G is the conductance, I is the current and U is the potential difference between the two junction electrodes. The current decays are accumulated to form linear and semi-logarithmic conductance histograms. The observed peaks in the conductance histograms correspond to the observed plateaus in the current decays and provide averaged single-molecule conductance values. An automated selection process designed by LabVIEW code was used to select the decays that showed plateaus from the ones that did not. The user defines the initial selection criteria that are fixed throughout all the experimental series. The yield of the decay curves showing plateaus was typically between 15 and 20% of the total collected curves. The bias voltage between the tip and substrate electrodes was set to −7.5 mV or +7.5mV depending the applied current sense direction.

The "blinking events" conductance values were obtained by capturing current transients at a fixed **Ni**-Au electrodes gap separation.[8,9] When the reactants are joined, an abrupt jump of the tunneling current in the form of telegraphic *blinks* is observed.[8,10–12] 2D maps were built by the accumulation of hundreds of these individual *blinks.* No selection procedures were applied to the data, so all blinking traces were used to build the histograms. In order to compare the lifetimes of the blinks in the 2D maps, all the captures were set into a common time origin and baseline.

5. Computational Details

5.1 DFT calculations of high and low spin states of the [NiDPP(p4m)$_2$] system system

The calculations were performed by optimizing the geometries for the S = 1 and S = 0 states with the Gaussian09 code (see Computational Details in the main text). We have employed the TPSSh functional because provides a better estimation of the state energies of transition metal complexes. The results indicate a small preference of 4 kcal/mol for the high spin state for the [NiDPP(p4m)$_2$] complex with pseudooctahedral coordination. It is well known the tendency of the Ni^{II} complexes to change from low-spin S = 0 state in square planar coordination mode to high-spin S = 1 in octahedral systems. In this case, we must to keep in mind that the position of the axial ligands is strongly affected by the interaction with the electrodes and such interaction can modify the subtle energy difference between the two states to stabilize the S = 0 ground state as found experimentally with the lack of magnetoresistance effect that is not consistent with the S = 1 high-spin state.

5.2 Transmission spectra for diamagnetic systems.

DFT calculations Siesta-Gollum PBE+U U = 4.0 eV

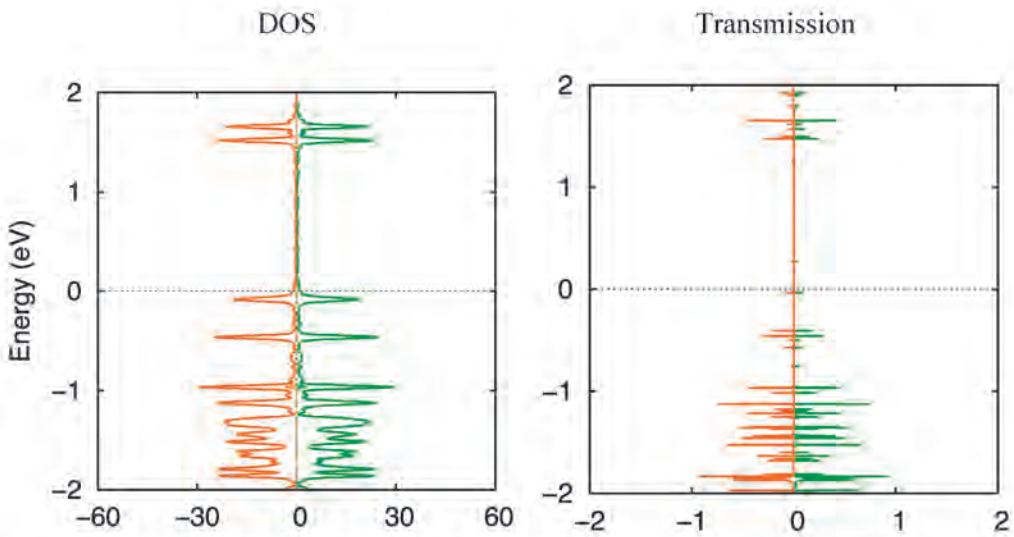

Figure S5.2 (left) DFT calculated DOS of the Co^{II} and Cu^{II} metalloporphyrins (filled curve corresponds to the transition metal levels) and (right) transmission spectra. Green and orange colors correspond to the alpha and beta spin contributions, respectively.

6. References

1. Aragonès, A. C. *et al.* Large Conductance Switching in a Single-Molecule Device through Room Temperature Spin-Dependent Transport. *Nano Lett.* **16,** 218–226 (2016).
2. Xu, B. & Tao, N. J. Measurement of single-molecule resistance by repeated formation of molecular junctions. *Science* **301,** 1221–3 (2003).
3. Chen, F. & Tao, N. J. Electron transport in single molecules: from benzene to graphene. *Acc. Chem. Res.* **42,** 429–38 (2009).
4. Zhao, Y. *et al.* Single-molecule spectroscopy of amino acids and peptides by recognition tunnelling. *Nat. Nanotechnol.* **9,** 466–473 (2014).
5. Inkpen, M. S. *et al.* New Insights into Single-Molecule Junctions Using a Robust, Unsupervised Approach to Data Collection and Analysis. *J. Am. Chem. Soc.* **137,** 9971–9981 (2015).
6. Li *et al.* Thermally Activated Electron Transport in Single Redox Molecules. *J. Am. Chem. Soc.* **129,** 11535–11542 (2007).
7. Hines, T. *et al.* Controlling formation of single-molecule junctions by electrochemical reduction of diazonium terminal groups. *J. Am. Chem. Soc.* **135,** 3319–22 (2013).
8. Aragonès, A. C. *et al.* Highly conductive single-molecule wires with controlled orientation by coordination of metalloporphyrins. *Nano Lett.* **14,** 4751–6 (2014).
9. Ponce, I. *et al.* Building Nanoscale Molecular Wires Exploiting Electrocatalytic Interactions. *Electrochim. Acta* **179,** 611–617 (2015).
10. Haiss, W. *et al.* Measurement of single molecule conductivity using the spontaneous formation of molecular wires. *Phys. Chem. Chem. Phys.* **6,** 4330–4337 (2004).
11. Aragonès, A. C. *et al.* Electrostatic catalysis of a Diels-Alder reaction. *Nature* **531,** 88–91 (2016).
12. Aragonès, A. *et al.* Detection of Single-Molecule Reaction Using STM Approach. *Protoc. Exch.* (2016). doi:10.1038/protex.2016.013

3.2.3 Findings and Discussion

— The main findings of this study were the following:

- *Tapping* experiments using non-polarized electrodes (non-magnetized Ni tips with Au substrate) did not show any difference on the current response under both current senses. Each metalloporphyrin show 3 current signatures associated to the contact geometries on different electrode-molecule binding sites. According to the results of the previous Section, the two low conductances values, associated to the interaction of the Ni tip-*Pyr* with the DPP *porphyrin ring* are equal for the four molecules as well as well as for the results for Co-DPP using Au tip electrode. The high conductance values, associated to the direct transport through metal is different for each central metal. The values according the following trend are Zn>Cu>Co>Ni.

- From the *tapping* experiments under *Au substrate-to-Ni tip* current, only the conductance values associated to the metal interaction for the paramagnetic metalloporphyrins Co-DPP and Cu-DPP, show spin-dependent behavior to the α-$\uparrow$Ni and β-$\downarrow$Ni tip polarization, the observed conductance changes are ca. 6-fold and ca. 4-fold, respectively. Under opposite Ni magnetic polarization conditions (*Ni tip-to-Au substrate*), the results showed a parallel scenario but with lower conductance variation being. 3-fold and ca. 2-fold, for Co-DPP and Cu-DPP respectively. Oppositely, under the same experimental conditions paramagnetic Ni-DPP and Zn-DPP did not show any dependence on the Ni tip polarization.

- *Tapping* experiments under *Au substrate-to-Ni tip* current sense performed in the absence of the *Pyr* at the Ni tip but with functionalized substrate electrode, suppress all the current signatures for Co-DPP, Ni-DPP, Cu-DPP metalloporphyrins For the Zn-DPP case the current signature associated to the metal was detected, and did not show any dependence to the Ni tip polarization.

- *Tapping* experiments employing tetra-phenilated DPPs and phenilated-free DPPs, showed two conductance signatures and one conductance signature respectively.

- *Blinking* experiments under *Au substrate-to-Ni tip* current, for the paramagnetic metalloporphyrins Cu-DPP show the same behavior observed for the equivalent *tapping* experiments under α-$\uparrow$Ni and β-$\downarrow$Ni tip polarization, but under $\perp$Ni polarizations the high conductance signature associated to the Ni tip-*Pyr*-metal interaction is suppressed

- *Blinking* experiments using non-polarized electrodes and under *Au substrate-to-Ni tip* current, show the same current behavior observed for the *tapping* experiments under the same conditions.

- *Tapping* and *blinking* experiments performed in the absence of metalloporphyrin molecules but with both Ni tip and substrate functionalized with *Pyr* groups and also the performed in the absence of the *Pyr* units at the Ni tip and substrate electrode but with Cu-DPP is present in solution, did not show any current signature

- Pulling curves collected during the selected *blinking* events showed plateaus. Contrary, the exerted on the tunneling current showed a sharp exponential current decay immediately after the application.

- DFT calculated conductance values show two different trends according a hexacoordinated metal center (two axial ligands) or pentacoordinated (one axial ligand), being respectively Co>Cu>Ni>Zn and Cu>Zn>Co>Ni.

- From the obtained Co-DPP and Ni-DPP calculations, the findings are the following. Co-DPP system has a *low-spin* S=1/2 electronic configuration ($d_{xy}{}^2 2_{xz}{}^2 d_{yz}{}^2 d_{z^2}{}^1 d_{z^2-y^2}{}^0$). The transported carriers are α-holes stated by the highest occupied α-d_{z^2} orbital which appears narrowly below the ε_F attesting their main contribution to the transport. Furthermore, Cu-DPP system has a *low-spin* S=1/2 electronic configuration ($d_{xy}{}^2 2_{xz}{}^2 d_{yz}{}^2 d_{z^2}{}^2 d_{z^2-y^2}{}^1$). The transport carriers are α-holes spin stated by the highest occupied α-$d_{z^2-y^2}$ orbital which appears narrowly below the ε_F attesting their main contribution to the transport. Ni-DPP DFT calculations results present a small energy difference between S=1 high spin and S=0 low spin states under octahedral coordination geometry.

— *The discussion of the results is summarized below:*

- MC and LC signatures can be associated to N-*Pyr* interactions witch the *porphyrin ring*, as confirm the control experiments performed using tetra-phenilated DPPs and phenilated-free DPPs. Such conductance signature can be associated to N-*Pyr* interactions with the *porphyrin ring* and with the phenyl rings connected to it, confirmed due the suppression of one of the two current signatures for the phenilated-free DPP case. Is important highlight that the conductance value difference between these two control experiments and the equivalent found for DPP are due the effect of the different number of phenyl group and the associated cooperatively *electro-donating* character, as previous studies confirms.[39,41,44,493,494]

- *Tapping* experiments in absence of *Pyr* units at the Ni tip, only shows current HC signatures for Zn-DPP. The obtained HC conductance value is equivalent to the HC signature obtained under both functionalized electrodes. Since the *Pyr*-free Ni tip scenario is associated to the pentacoordination of the metal, and the functionalized electrodes case is due the hexacoordination, indubitably the Zn-DPP is coordinated by former way.[456] Despite the pentacoordination, the observed a high conductance range is equivalent to the other studied Co, Ni and Cu metalloporphyrins, and can be justified through a metallic interaction between the electrodes and the Zn-DPP though the porphyrin ring[495,496] or the metal center.[496–498] The metalloporphyrins pentacoordination also avoids the interaction with the DPP *porphyrin ring* since the suppression of low conductance current signature due the absence of N-pyr *Pyr* to the Ni tip and their interaction with the porphyrin ring.

- *Blinking* measurements of Cu-DPP under *Au substrate-to-Ni tip* current, attest the lack of effects due the molecular stretching in any measurement.

- Pulling curves collected over the blinks, showed large plateaus analogous to the current signatures associated to the different binding sites of electrode-molecule, the other small plateaus are due the molecular stretching. This attest the establishment of the molecular junctions.

- Despite the well-know DFT methods' drawbacks to reproduce quantitatively the experimental data as well as the lack of an accurate structure of the tip–molecule–substrate system in the exact moment that the measure is performed,[365–367] the obtained conductance values reproduce qualitatively the trend of the increasing conductance for the Ni-DPP, Cu-DPP and Zn-DPP molecules, using the hexacoordination for the Cu-DPP and Ni-DPP and pentacoordination for the Zn-DPP, according to the experiential results. However, the obtained value for Co-DPP show a excessively higher conductance value. Despite is not according to the experimental results the calculation has been performed employing the d_{z^2} orbital since is the related with main channel responsible of the spin-dependent transport. Is important to highlight that

any small change in the M-N distance from the equilibrium, in the interaction with the STM tip could cause significant changes in the obtained calculated values, i.e such values provided by the DFT are very sensitive to small changes under the employed model to perform the calculations.

- From the obtained calculations, is proved that Cu-DPP and Co-DPP cases show different effective channels for α-$\uparrow$ and β-$\downarrow$ carriers and justifies the MR effect because the narrowly energy difference between the ε_F and the highest occupied Co-DPP (α-$\uparrow$)-d_{z^2} and Cu-DPP $d_{z^2-y^2}$ orbitals, resulting in a conduction through majority holes (α-$\uparrow$)-carriers for both Co-DPP and Cu-DPP cases. On the contrary, Ni-DPP and Zn-DPP are not suitable for spin-filtering. Despite Ni-DPP is an paramagnetic molecule, such as DFT confirms due the energy difference between S=1 *high-spin* and S=0 *low-spin* states, the no-dependence on the Ni tip polarization could be explained by the presence of *low-spin* Ni(II) centers[366] Zn-DPP since is a closed-shell molecule was not expected any dependence effect on the Ni-tip polarization.[151,188,189,288,289,295–298]

- According to the model, single-current measurements experiments under magnetized Ni tips, show MR effects for Co-DPP and Cu-DPP under *Au substrate-to-Ni tip* consequence of the α-$\uparrow$ pre-polarization of the carriers to the Spinterface and the subsequent injection to the Co-DPP or Cu-DPP molecules, which are parallel aligned according the Ni tip polarization direction and depending the molecular magnetic moment's orientation and the associated spin preferences the current will be tuned. Since the majority spin-carrier preferences for Co-DPP and Cu-DPP, the spin-polarized current will be blocked by the metalloporphyrin under a the β-$\downarrow$ Ni and fully transmitted at α-$\uparrow$Ni. The Ni tip represents the last step for the MR tuning since its minority spin-carriers preferences, thus the α-$\uparrow$ pre-polarized current injected from the metalloporphyrin will be blocked under α-$\uparrow$Ni or fully transmitted under β-$\downarrow$Ni.

- According to the model, single-current measurements experiments under magnetized Ni tips, show MR effects for Co-DPP and Cu-DPP under *Ni tip-to-Au substrate*. The minority spin-carriers preferences of the Ni tip causes the injection of polarized current depending on its polarization, under α-$\uparrow$Ni injects β-$\downarrow$ pre-polarized current and under β-$\downarrow$Ni injects α-$\uparrow$ polarized current. Once such pre-polarized current is injected to the metalloporphyrin, the current will always be blocked because the metalloporphyrins magnetic moment is parallel aligned according the Ni tip polarization and also due the opposite spin-carrier preferences for both subsystems, however the observed MR between α-$\uparrow$Ni and β-$\downarrow$Ni tip polarization directions can be ascribed to the inherent Spinterface's preferences according to the proposed qualitative model.

- The spin-dependent transport (current blockage) caused by the perpendicular magnetization of the Ni tip can be justified as a blockage of the channels with large orbital participation of the paramagnetic centers. Further research is needed.

3.3 Conclusions of the Chapter

In this chapter, has been develop a novel concept of single-molecule platforms employing the STM at RT based on metalloporphyrins and mimicking their natural configuration orienting the molecular plane perpendicular to the electron-pathway. To achieve it, was established a junction via the axial coordination of the metal center by chemically modifying both STM tip and surface electrodes with pyridin-4-yl-methanethiol. Thanks to "axially trapping" the metalloporphyrin molecule, a new flat conformation is available, since the metal center is hexacoordinated causing a highly stable molecular wire which makes possible the electronic conduction through inaccessible pathways to the date for single-molecule contacts employing similar metalloporphyrin molecules, but wired from either end of the porphyrin ring. It has been demonstrated that the metal incorporation to the porphyrin rings is the origin of the specific new electron-pathways. For the studied metals Co, Ni, Cu and Zn introduced in the porphyrin rings was achieved a molecular conductance of three orders of magnitude larger than that obtained in previous works. The significant increased molecular-conductance attests the improved efficiency for the electron-pathway via an electron transport directly through the metal, and the consequent significant reduced resistivity since the porphyrin ring environment is not involved,[376,419] therefore providing a unique assembly of highly conductive single-molecular wires.

The new electron-pathway through the metal center also presents spin- dependence, behavior according to the spin-filtering capabilities of the employed metal, like Co-DPP and Cu-DPP cases which present different effective α or β channels for the spin-carriers since gather the required conditions explained at Chapter 2: occupied polarized orbitals strongly interacting with the junction metal electrodes jointly with close energy values to the ε_F for one of the two spin-carriers (holes) allowing the electron transport though it. Consequence of the established electronic properties for Co-DPP and Cu-DPP junctions, is obtained an intermediate MR effect between opposite Ni α-$\uparrow$Ni and β-$\downarrow$Ni injects α-$\uparrow$ polarizations of approx. 6-fold. Also, the obtained molecular conductance values represent the largest values reported for a magnetoresistive molecular-device based on metalloporphyrins. Furthermore, through a perpendicular-to-the-metal polarized current, the transport is fully blocked therefore showing a huge anisotropy, representing a MR benefice of 100-fold close to the obtained by the metal complexes of the previous chapter, allowing to the system to behave as a switch too.

The presented new platform also allows by tuning the STM tip-surface distance, the controlled modification of the junction via reconfiguring the metalloporphyrin-electrodes binding sites. Consequence of the not allowed axial metal coordination at intermediate and large electrodes separation, different tilted conformations are promoted through H-bonding between the porphyrin ring and the functionalized electrodes. As a direct consequence, the conductance output of the single-molecule device is affected since such configurations present a significant lower molecular conductance up to ca. one order of magnitude, respect the offered by the flat conforma-

tion. This is because in such tilted conformation the electron-pathway is established through the backbone without any interplay with the metal thus offering a less efficient conduction.[499] Such non-dependence on the metal centers is attested by the equivalent LC and MC conductance values showed by all the different metalloporphyrins as well as by the metal-free porphyrin ring. Another noteworthy implication of the non-correlated electron-pathway, is the suppression of the spin-dependent effects of the conductances associated to the tilted configurations, consequence of the spin-filtering strong dependence on the metal centers already demonstrated in the previous chapter. Such spin-dependence suppression as a consequence of attachment at multiple binding sites and the caused different molecular orientation, have been theoretically studied in several previous works,[484,500–503] being many of them about metalloporphyrin.[502,503]

The presented MR behavior on the single-metalloporphyrin junction, was designed by employing the *key-parameters* deduced from the previous chapter (***Spinterface***, Ni tip ***magnetic polarization*** and ***closed-shell electronic structure*** for the central molecule) and consequently presents the same qualitative model. However, exist three significant differences with the prior. *(i)* The intermediate MR efficiency compared to the highly presented by metal complex molecules junctions, *(ii)* the midway conductance values for the non-magnetized Ni tip compared to the polarized cases and also *(iii)* the unexpected MR effect presence under *Ni tip-to-Au substrate* sense, which suppresses the "spintronic diode" effect observed in the metal complexes junctions. The metalloporphyrins preferences for the majority spin-carriers opposite the presented by the Ni tip, justify the three observed unexpected effects:

1. As a result of the mismatching between the spin-carriers preferences presented by the metalloporphyrins (majority spin-carriers favored) and the Ni tip (minority spin-carriers favored) the spin-polarized carriers cannot be completely blocked or fully transmitted, because always one of the two subsystems will present an electronic structure unfavorable to the injected polarized current, therefore causing an energy penalty to the unfavored spin-carriers, meanwhile the other ingredient will present the opposite behavior suppressing any energy penalty. This is translated to a significant reduction of two orders of magnitude for the MR efficiency presented by metalloporphyrins junctions versus the presented by metal complexes.

2. In the previous single-molecule devices based on metal complexes, there was a permanent *minority* α-(pre)polarized current which dominates the conducting state of the paramagnetic junction injecting from the Au surface to the molecules, which explains the high MR efficiency and the common conductance value between all the measurement with detectable current. But for the showed junctions of this chapter, the suppression of such conducting stage domain can be hypothesized due the weaker SOC effects presented by the metalloporphyrins particualry as a consequence of the used anchoring group.[344] Such hypothesis cannot be validated and assuming that the non-magnetized

Ni tips are the average of all the polarizations contributions at the same time, the emerged scenario hinders any possible explanation of the model at this early stage of development. Another explanation can be related on the high resistivity presented by the metal complexes conductances causing an indistinguishable conductance variation. Regardless the reason, it needs further research form the theoretical point of view.

3. The Ni tip–molecule alignment due Zeeman effect, which aligns the metalloporphyrin magnetic moment in its low-energy configuration,[285,286] combined with the above explained spin-carrier mismatching, represent the reason to observe the MR effect also under a positive bias (*Ni tip-to-Au substrate* sense). Mainly, the Ni tip never will inject to the metalloporphyrin the preferred spin-carrier population of the latter, thus permanently will be a blocking current effect on the Ni tip-molecule interface imposing an energy penalty to the transmitted (and always unfavored) polarized carrier, therefore impeding the MR effect suppression observed by the metal complexes junctions. Nonetheless, the observed MR effect under both current senses is not equivalent, being higher the MR ratio presented by the *Au substrate-to-Ni tip* analogous to the observed with metal complexes junctions. Such asymmetry can be justified by the dissimilarity of the metal electrodes and their natural differences on the surface states as some studies suggest.[318,504]

As a final comment, highlight the two major challenges which can be extracted from the development of the presented single-molecule device: the need to go further in the exploration on coexistent electronic-pathways in the same molecule but presenting different dependences on a metal and its associated properties, like the spin-filtering capabilities; as well as, the need to expand the research based on the transport of spin-carriers perpendicularly polarized to the electrical current, given the outstanding efficiency of the observed MR effect compared with the other employed polarization directions.

A part from the mainly conclusions related with the new developed platform and the studied spin-dependent transport, below, are summarized other notable conclusions extracted from the research:

- The MC and LC signatures, associated to the interaction between the porphyrin ring and the functionalized electrodes despite were useful to discern between the established electron-pathways and the spin-dependent current, in a real single-molecule device should be avoided. It can be done employing different porphyrin rings with electron-withdrawing substituents[41] aiming to lower its conductance as attest the control experiments with tetra-phenilated DPPs and phenilated-free DPPs. Besides, the independent electron-pathways between the metal and the porphyrin ring, can be assumed that the incorporation of withdrawing substituents will mostly affect the conductance associated to the porphyrin ring.[499] The structural modification consequence of the axial

trapping of the metal centers, results on the transition from tetracoordination to hexacoordination. It explains the increment of the molecular conductance level observed for the presented junctions. Such conductance values are in agreement with the presented by previous works employing molecular wires based on metallorganic redox structures inserted into a molecular backbone.[505,506] Even so, such argument lacks for the Zn-DPP case, a well-known cation to present preferentially pentacoordination[456] and also proved experimentally with the control experiments, although keeps the flat conformation thanks the electrode–Zn-DPP interaction through the metal center[496–498] or via porphyrin ring.[495,496] This strongly suggests that the pillar for the highly conducting molecular wires could be merely due the molecular plane position respect the electron-pathway as long as exists a strong enough interaction with the electrodes. Further research is needed to find it out. Regarding the highest conductance values presented for the Zn-DPP molecule, can be justified since the shortened electron-pathway compared to Co-DPP, Ni-DPP and Cu-DPP cases, due the presence of only one axial ligand which reduce the electrodes distances.

- In this chapter, is possible to distinguish the role of each penalty, as is exemplified in the *Au substrate-to-Ni tip* current sense, where each penalty is showed individually. Thus, can be extracted that the penalty associated to the molecule's spin preferences (under β-$\downarrow$Ni polarization) is more significant that the presented by the Ni tip (under α-$\uparrow$Ni polarization) since the difference of the measured conductance. The observed trend is according to previous studies employing metalloporphyrins introducing the same transition metal centers but using the up-right conformation.[300] As previous theoretical studies proposed, due the interplay between such electron-pathways with the metal center, the molecular wire conductance can be tuned according the metal used binding energy.[507]

- Despite the presented MR efficiency is lower compared to the presented by the metal complexes, in the presented junctions since the different spin-carrier preferences of the Ni tip and the metalloporphyrin molecules, is possible to tune the current in different conductance levels, achieving a kind of "Spintronic variable resistor" controlled by the Ni tip polarization direction and the current sense (applied bias), instead of the switching capabilities offered by the preceding single-molecule devices based in metal complexes. However, the perpendicular polarization of the Ni tip enables the junction to completely block the electron-pathway through the metal center increasing the conductance tunability of the single-molecule device, supplementing it with the switching behavior. Regardless of the long-term possible applicability, the tunable current effects presented by the current single-molecule device can be achieved at a near-zero bias voltage, thus the junction presents a low power consumption since the MR effect are significant considering the small currents worked with.